Imaging of Infection in the Diabetic Foot

6

Mary G. Hochman

Abstract

Information derived from imaging studies can play an important role in the management of complicated foot problems in the diabetic patient. This chapter reviews the various modalities available for imaging of the diabetic foot—radiography, nuclear medicine studies such as bone scanning, labeled leukocyte scans, gallium, and Flourine-18-flourodeoxyglucose positron emission tomography (FDG PET) scans, cross-sectional studies such as magnetic resonance imaging (MRI), CT, and ultrasound, and various forms of angiography—and highlights their relative strengths and weaknesses for the diagnosis of osteomyelitis, soft tissue infection, and neuroarthropathy. A suggested imaging algorithm for the diagnosis of osteomyelitis in the diabetic foot is presented.

Keywords

Diabetic foot • Osteomyelitis • Neuroarthropathy • Imaging studies • Bone scan • Labeled leukocyte scan • Gallium scan • MRI • CT • US • Angiography

Introduction

Foot infections are among the most common causes of hospitalization in the diabetic population, accounting for 20% of all diabetes related admissions. Complicated foot infections may require treatment by amputation—as many as 6–10% of all diabetic patients will undergo amputation for treatment of infection [1–3], accounting for 57% of nontraumatic lower extremity amputations [4–6]. The scope of the problem is compelling. Infections and complicated vascular diabetic foot problems result in 50,000 amputations a year in the USA [7]. The Centers for Disease Control and Prevention (CDC) estimated the annual treatment cost of amputees within this group at $1.2 billion for the year of 1997. However, this figure does not include the cost of rehabilitation, prosthetic devices, or lost income. These treatment costs are likely to grow, as the prevalence of diabetes is on the rise. A recent

M.G. Hochman, MD, MBA (✉)
Musculoskeletal Imaging Section, Beth Israel Deaconess Medical Center, Harvard Medical School,
330 Brookline Avenue, Boston, MA 02215, USA
e-mail: mhochman@bidmc.harvard.edu

A. Veves et al. (eds.), *The Diabetic Foot: Medical and Surgical Management*, Contemporary Diabetes,
DOI 10.1007/978-1-61779-791-0_6,

epidemiology study shows an increase of the overall prevalence of diabetes from 12.1 million in 2002 to 17.5 million in 2007 [8].

Information derived from imaging studies can play an important role in management of complicated foot problems in the diabetic patient. Soft tissue abnormalities such as abscesses and cellulitis can be identified, osteomyelitis can be detected, the extent of abnormal marrow can be depicted, neuroarthropathic changes can be diagnosed and followed over time, distribution of atherosclerotic lesions can be mapped, and the effectiveness of re-vascularizaton procedures can be evaluated. A variety of studies are currently available for imaging the diabetic foot. In order to use these imaging studies effectively, it is important to understand the specific strengths and weaknesses of each modality, as they apply to the particular clinical problem in question. The goal of this chapter is to review the modalities available for imaging of diabetic foot infection and to highlight their relative utilities in the context of clinical problem solving.

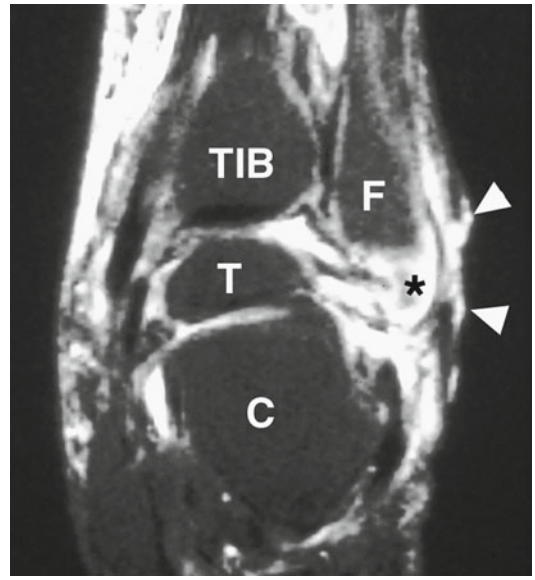

Fig. 6.1 Osteomyelitis deep to ulcer on MRI. Coronal fluid-sensitive STIR image of the left foot of a diabetic patient shows an area of marrow edema (*asterisk*) at the tip of the fibula (F). Overlying this focus of abnormal marrow is an ulcer surrounded by diffuse soft tissue swelling (*arrowheads*). These findings represent osteomyelitis of the distal fibula. *C* calcaneus, *TIB* tibia, *T* talus

Infection in the Diabetic Foot

Risk Factors

Many factors contribute to infection in the diabetic foot, including peripheral neuropathy [9] and vascular insufficiency [10]. Repetitive minor trauma to an insensitive neuropathic foot, exacerbated by abnormal biomechanics or ill-fitting shoes, causes areas of increased plantar pressure to develop callus, which, in turn, predisposes to ulcer development. Clinically occult ulcers form insidiously, deep to the callus [11, 12]. Direct extension of infected ulcers or soft tissue infection to bone leads to osteomyelitis [13] (Fig. 6.1). These infections are usually polymicrobial and involve both anaerobic and aerobic pathogens.

Soft Tissue Abnormalities

Soft tissue abnormalities associated with the diabetic foot include soft tissue edema, cellulitis, soft tissue abscess, ulcers, sinus tracts, tenosynovitis, joint effusions, and arthritis [14–16]. The importance of differentiating these conditions lies in their differing management: abscess necessitates prompt surgical drainage, septic arthritis requires surgical debridement, and cellulitis generally entails antibiotic therapy.

Soft tissue edema and swelling is a common finding in the diabetic patient. Soft tissue swelling can occur in the absence of infection, due to vascular insufficiency or peripheral neuropathy (Fig. 6.2) [16]. However, soft tissue swelling can also reflect the presence of cellulitis, that is, soft tissue infection of the superficial soft tissues. Cellulitis along the dorsum of the foot usually occurs secondary to surface infections in the nails, toes, or Web spaces. Simple cellulitis is generally diagnosed clinically, without the need for imaging. The major indication for imaging of patients with cellulitis is suspected underlying deep infection, such as soft tissue abscess, osteomyelitis, or septic arthritis.

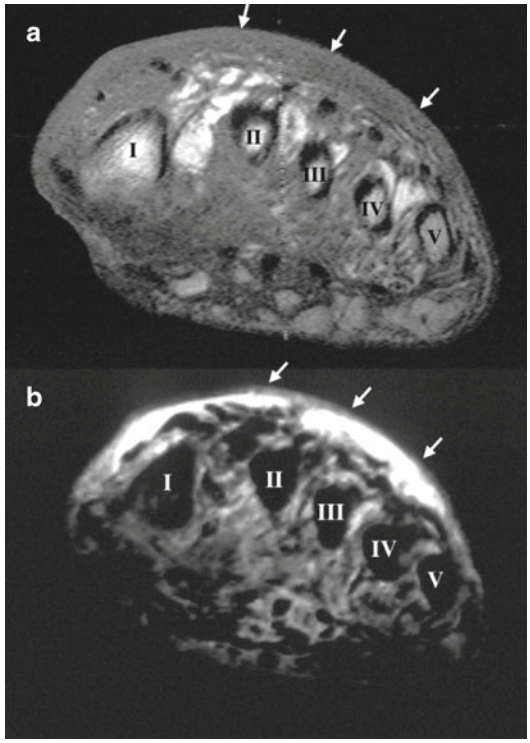

Fig. 6.2 Dorsal soft tissue swelling on MRI. (**a**) T1-weighted image and (**b**) fluid-sensitive STIR image are coronal or short axis images acquired at the level of the mid-metatarsal shafts. This diabetic patient has diffuse dorsal soft tissue swelling (*small arrows*). The subcutaneous edema is dark or low signal on the T1-weighted image and bright or high signal on STIR. Note the presence of normal fatty marrow signal in the metatarsal bones—high signal (*bright*) on T1 and low signal (*dark*) on STIR, conclusively ruling out osteomyelitis. *I–V* first to fifth metatarsals

Osteomyelitis

Osteomyelitis of the foot occurs up to 15% of diabetic patients [15]. Bone infection results from local extension of soft tissue infection (Fig. 6.1). Callus and ulcers serve as the conduits for infection to spread to deep soft tissue compartments, bones, and joints. The most common sites of soft tissue infection and secondary osteomyelitis are foci of increased plantar pressure, such as the metatarsal heads and the calcaneus (Fig. 6.3). Evaluation of foot ulcers is important because more than 90% of osteomyelitis cases result from contiguous spread of infection from soft tissue to bone [7]. Newman et al. further demonstrates a clear relationship between ulcer depth and osteomyelitis: 100% of ulcers exposing bone and 82% of moderately deep ulcers were shown to have osteomyelitis on bone biopsy [1] (Fig. 6.1).

Identification of osteomyelitis in the diabetic foot can be difficult both clinically and radiographically. Ability to probe a pedal ulcer through to bone (Fig. 6.3) has been reported as a useful index of underlying osteomyelitis in a diabetic patient [17] and is commonly used to guide decisions regarding treatment. Nonetheless, clinical judgment was shown to be a poor indicator of infection. The technique of probing to bone, only 68% sensitive, may underestimate the incidence of bone involvement, according to Newman et al. [1]. In the same study, 18 out of 19 of pedal ulcers did not expose bone nor display inflammation, yet contained osteomyelitis. Moreover, other clinical parameters such as fever and leukocytosis are unreliable in the diabetic patient. For example, in a study by Bamberger et al., only 18% of patients with clinically severe osteomyelitis were febrile [13]. Neither fever nor leukocytosis predicts the necessity for surgical exploration [18].

Imaging Modalities

Imaging can play a role in diagnosing and distinguishing between bone and soft tissue infection, characterizing soft tissue abnormalities, identifying osteoarthopathy and other bony abnormalities, and mapping vascular disease for surgical intervention. A variety of imaging modalities can be useful in the evaluation of the diabetic foot, include radiography, scintigraphic examination, CT, magnetic resonance imaging (MRI), US, and angiography. Imaging techniques vary in their sensitivity for detection of osteomyelitis, with specificity limited in the presence of cellulitis, peripheral ischemia, and diabetic neuropathic osteoarthropathy [19, 20] (Table 6.1). In the appropriate setting, however, noninvasive imaging can aid in diagnosis and treatment planning.

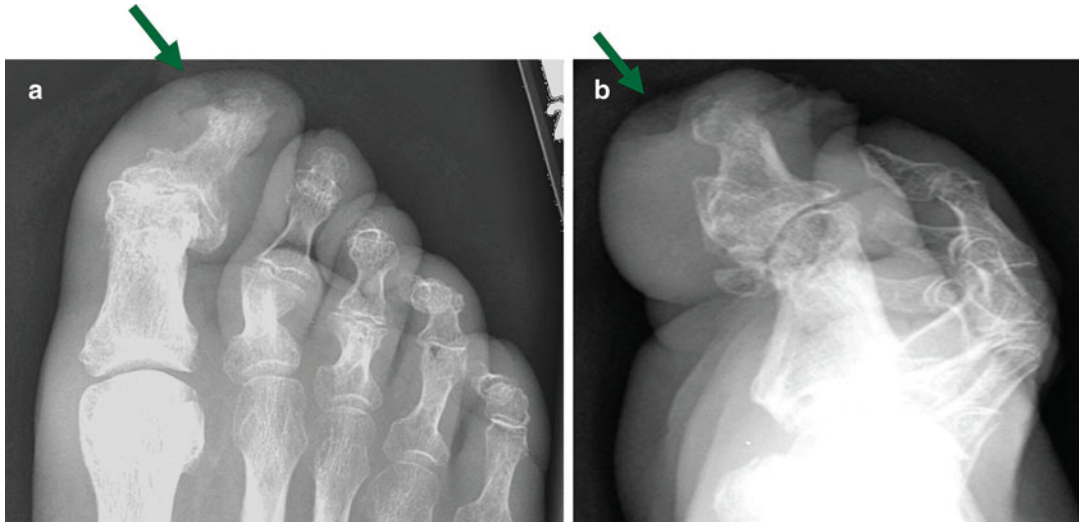

Fig. 6.3 Osteomyelitis of first distal phalanx. (**a**) AP and (**b**) lateral views of the great toe show an ulcer (*arrow*) overlying the distal phalanx. The cortex of the bone is indistinct and there is underlying osteopenia, representing osteomyelitis. On clinical examination, exposed bone was evident at the ulcer

Table 6.1 Compilation of sensitivity and specificity of various imaging modalities in the diagnosis of osteomyelitis

	Range of sensitivity (%)	Range of specificity (%)	Compiled sensitivity/specificity (%/%)	References
Radiography	52–93	33–92	61/72	[26, 27, 31, 80, 82, 83, 102, 126–128]
Three-phase bone scan in patients without bone complications			94/95	[23] Review of 20 published reports
Three-phase bone scan in patients with bone complications			95/33	[23]
In-111 labeled WBC	75–100	69–100	93/80	[26, 27, 31, 129]
Combined gallium and bone scan			81/69	[23]
MRI	29–100	67–95	96/87	[80–84, 129]

Radiographs

Radiography ("X-ray") remains the first screening examination in any patient with suspected infection and have the advantage of being inexpensive and easily obtainable. Radiographs can help to identify an unsuspected diabetic patient by demonstrating calcification in the interdigital arteries: these vessels rarely calcify in nondiabetic patient [21]. Cellulitis results in increased density and thickening of the subcutaneous fat, though nonspecific soft tissue edema can have a similar appearance. Both bone and soft tissue infection can result in blurring of usually visible fat planes. Focal fluid and callus both demonstrate focal increased density in the subcutaneous fat. Ulcers may or may not be visible on radiographs, depending on their size and orientation. (Fig. 6.5). In general, all of these soft tissue abnormalities are more clearly evident at physical examination. However, radiographs do readily depict subcutaneous emphysema associated with infection or recent surgery (Fig. 6.4). Some foreign bodies, i.e., denser materials such as

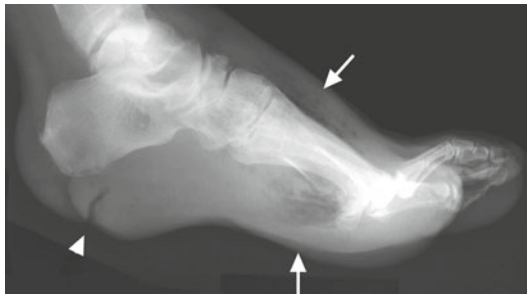

Fig. 6.4 Soft tissue air and deep ulcers on radiography. The lateral view of the right foot from a diabetic patient shows subcutaneous air (*arrows*) in both dorsal and plantar soft tissues surrounding the metatarsals. A deep ulcer dissects into the heel fat pad (*arrowhead*)

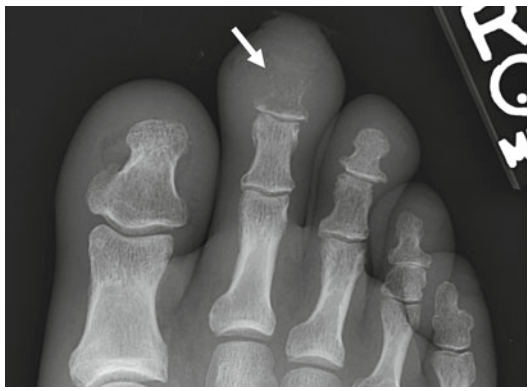

Fig. 6.5 Osteomyelitis of the second distal phalanx. Extensive destruction of cortical and medullary bone (*arrow*), with surrounding soft tissue swelling

metal and lead-containing glass are radio-opaque and generally are visible on radiographs. In order to detect nonmetallic foreign bodies and subtle soft tissue calcifications, radiographs acquired with "soft tissue" technique (i.e., lower kV than a routine radiograph) may be required.

Findings of osteomyelitis on radiographs include soft tissue swelling and effacement of tissue fat planes, permeative medullary radiolucency, focal osteopenia or focal osteolytic lesion, periosteal new bone formation, endosteal scalloping, and cortical bone destruction (Table 6.2; Figs. 6.3–6.5). Of note, these osseous changes typically only become apparent after osteomyelitis has been present for 10–14 days and require up to 50% bone loss before becoming evident on a radiograph [22]. Comparison to prior films, when available, can help to highlight early changes. In the majority of studies, sensitivity of radiographs ranges between 52 and 93% and specificity ranges between 33 and 92%, for detection of osteomyelitis (Table 6.1). When radiographs are positive for osteomyelitis, further imaging studies are often not required. However, radiography is less sensitive compared with other imaging modalities and a negative X-ray examination does not exclude osteomyelitis. Moreover, radiographs are not sensitive for detection of soft tissue infection, such as septic arthritis or abscess formation.

Table 6.2 Radiographic findings of acute osteomyelitis

Soft tissue swelling and effacement of soft tissue fat planes
Permeative medullary radiolucency
Focal osteopenia or focal osteolytic lesion
Periosteal new bone formation
Endosteal scalloping
Cortical bone destruction

Even when radiographs do not demonstrate findings of osteomyelitis, they nonetheless play an important role in the diagnostic-work-up of infection. Because they demonstrate changes of neuroarthropathy, postsurgical changes, fractures, foreign bodies, gas, foot deformities, and bony variants, radiographs can serve as roadmaps for other imaging examinations. In the absence of correlative radiographs, these findings can cause unnecessary confusion on MRI or nuclear medicine examinations.

Nuclear Medicine

The three most commonly employed nuclear medicine or scintigraphic tests for the diagnosis of diabetic foot infection are bone, labeled leukocyte scans, and gallium scans. FDG PET has shown utility for diagnosing musculoskeletal infection, but is not yet routinely reimbursed for this indication. Bone, labeled leukocyte, and gallium scans are all considered highly sensitive to the presence of both soft tissue infection and

osteomyelitis (Table 6.1). When the foot is radiographically normal, bone scan is the scintigraphic examination of choice. When preexisting bone changes are present (i.e., neuroarthropathy, trauma, degenerative changes), labeled leukocyte scan provides the best overall sensitivity and specificity among the nuclear medicine studies (Table 6.1).

Bone Scan

Traditionally, triple phase bone scan (TPBS) has been the test used for the work-up of suspected osteomyelitis in patients with negative radiographs. It is widely available and easy to perform. A three-phase bone scan involves intravenous injection of radioactive technetium-99m methylene diphosphonate, followed by imaging with a gamma camera at three distinct time points. Images acquired every 2–5 s immediately following injection provide a radionuclide angiogram (the flow phase) and may demonstrate asymmetrically increased blood flow to the region of interest. The tissue or blood pool phase is obtained within 10 min and reveals increased extracellular fluid seen in conjunction with soft tissue inflammation. A delayed, skeletal phase is acquired 2–4 h after the injection. The skeletal phase demonstrates areas of active bone turnover, which have incorporated the radionuclide tracer, and are seen as focal "hot spots" of increased tracer activity. The tracer is taken up by bone in an amount dependent on both the degree of osteoblastic activity and the blood flow to the area. In some facilities, single-photon emission computer tomography (SPECT) spanning can be performed in conjunction with a technetium bone scan to generate tomographic, cross-sectional images of radionuclide activity that can be reformatted into different planes and can help to clarify problems created by bony overlap. Because SPECT images have greater intrinsic contrast than routine planar images, the SPECT images are also more sensitive in detecting foci of radionuclide activity.

Osteomyelitis results in increased uptake in all three phases of a bone scan, whereas simple cellulitis demonstrates increased uptake in the first two phases only (flow and tissue or blood pool phases) (Fig. 6.6). In cellulitis, there may be mild diffuse increased uptake in the bone due to inflammation, but this is distinct from the more focal, intense increased uptake seen with osteomyelitis. However, uptake in the delayed phase itself is not specific for osteomyelitis. In general, a positive delayed phase scan is seen when there is an underlying process that promotes bone remodeling, e.g., healing fracture, neuropathic osteoarthropathy, or recent bone surgery. False negatives may occur when the radiotracer fails to reach the foot because of diminished vascular flow. This is of particular concern in diabetics with atherosclerotic disease.

Schauwecker's review of 20 published reports shows a compiled mean sensitivity and specificity of 94% and 95%, respectively, for detection of osteomyelitis with bone scintigraphy [23]. Unfortunately, this data applies only to patients without underlying bone deformities. In the diabetic patient with complicated bone conditions such as recent fractures and neuroarthropathic changes, a common clinical presentation, the sensitivity remains at 95%, but the specificity declines to 33% [23]. Thus, the American College of Radiology (ACR)-sponsored appropriateness criteria for detection of osteomyelitis recommends a three-phase bone scan only when radiographic findings of bone complications are absent [24]. If radiographic findings of bone complications are absent and the bone scan is normal, then there is little likelihood of osteomyelitis and the investigation can be considered complete. However, when the radiograph reveals an underlying focal bony abnormality, then a bone scan is unlikely to be definitive and, therefore, a labeled leukocyte study or MRI is recommended instead. If a labeled leukocyte scan or MRI is not available, a gallium scan may provide a useful alternative.

Labeled Leukocyte Scan

Labeled leukocyte scans, also known as labeled white blood cell (WBC) scans, are the preferred scintigraphic technique for imaging when there is background bone pathology on radiographs. This is because WBCs accumulate at sites of infection, but, unlike bone scans, they do not accumulate at sites of increased bone turnover, such as

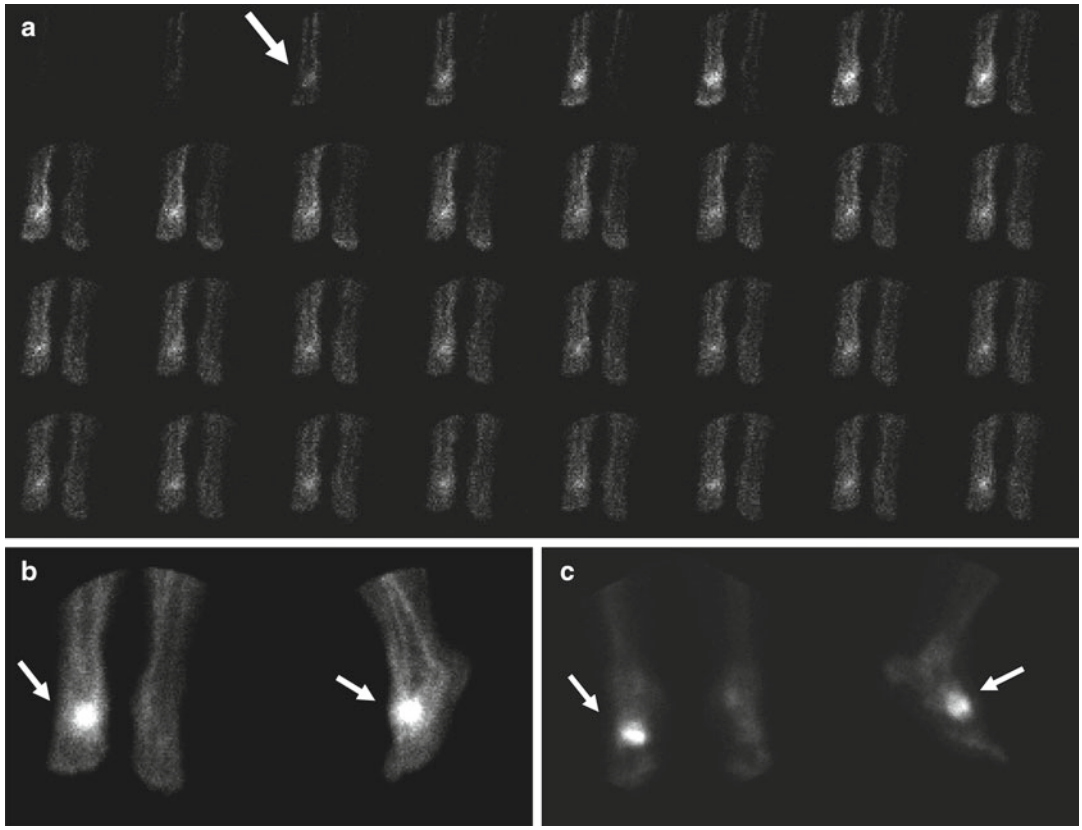

Fig. 6.6 Osteomyelitis on triple phase bone scan (TPBS). (**a**) Radionuclide angiogram (flow phase) of a TPBS with successive images obtained every 2–5 s following injection, showing asymmetrically increased blood flow to the distal right lower extremity (*arrow*). (**b**) Blood pool phase obtained within 10 min after injection shows increased activity in the right foot (*arrows*), reflecting increased extracellular fluid related to soft tissue inflammation. AP view on the left and lateral view on the right. (**c**) Delayed skeletal phase acquired 2–4 h after injection shows increased activity in the bones of the midfoot. In this phase, "hot spots" reflect areas of active bone turnover (*arrows*) and is therefore specific for bone. Note that the signal seen in the soft tissues on the preceding blood pool phase has cleared. AP view on the *left* and lateral view on the *right*

fractures and neuropathic osteoarthropathy. WBC scans are performed by extracting a patient's blood, fractionating the leukocytes from blood, incubating the WBCs with either indium 111-oxine or technetium-99m-hexamethylpropylene amine oxime (Tc-HMPAO) in order to label them, and then re-injecting the labeled WBCs into the same patient. Imaging is performed 16–24 h later, using a standard gamma camera. As noted above, labeled WBCs theoretically only accumulate at sites of infection and not at sites of increased osteoblastic activity and therefore should be extremely useful in the diagnosis of complicated osteomyelitis (Fig. 6.7). The technique is most useful for inflammatory processes that are mediated by neutrophils, such as bacterial infections, since the majority of leukocytes labeled are neutrophils [25]. In addition, a total white count of at least 2,000/μL is needed to obtain satisfactory results [25].

Indium-labeled leukocyte scan offers the best sensitivity and specificity among the three readily available scintigraphic techniques (Table 6.1). A compilation of seven studies yielded a sensitivity of 93% and specificity of 80% [1, 26–31]. In addition, Newman suggested that indium-labeled leukocyte imaging could be used to monitor response to therapy, with images

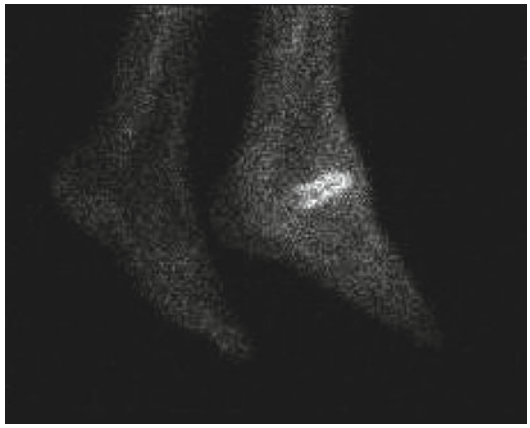

Fig. 6.7 Osteomyelitis on indium-labeled leukocyte scan. Increased indium accumulation about the ankle represents a focus of osteomyelitis in a patient with swelling and fever. Staph aureus grew from the marrow aspirate

reverting to normal 2–8 weeks after commencement of antibiotic therapy [1].

Despite their potential advantages and reported high sensitivity and specificity, indium-labeled leukocyte scans have not completely displaced other imaging modalities. Recent data shows false-positive uptake of indium-labeled leukocytes in as many as 31% of noninfected neuropathic joints [32]. These false-positive examinations stem from the inability to determine whether labeled leukocytes located outside the typical marrow distribution represents infection or merely an atypical site of hematopoietic activity [33]. Atypical patterns of marrow distribution may accompany fractures, orthopedic hardware, infarctions, systemic diseases, and tumors. At sites where bone marrow may be present, it is very helpful to compare the leukocyte scan with a bone marrow scan obtained with technetium-99m-macroaggregated albumin. False-negative examinations may occur when the procedure for labeling the leukocytes is inadequate [34]. Detection of osteomyelitis is rarely a problem in the forefoot, where the osseous structures are equidistant from both dorsal and plantar skin surfaces, but may be compromised in the mid- and hindfoot due to anatomic complexity in these areas [33]. Interpreting the labeled leukocyte study in conjunction with the anatomic localizing information available from a simultaneously acquired bone scan can help to improve accuracy [31].

Technitium-99m HMPAO-labeled leukocyte scans are reported to be as accurate as indium-labeled leukocyte studies in the diagnosis of osteomyelitis. This technique of labeling has the advantage of providing the results on the same day and depositing a much lower radiation dose. Its major drawback is that it does not permit simultaneous acquisition with bone or bone marrow scans.

Other disadvantages associated with both indium- and technetium-99m HMPAO-labeled leukocyte scans include the complexity of the labeling process, high costs, limited availability of the test, and the risks inherent in handling of blood products. Because of the difficulties inherent in in vitro labeling of leukocytes, several techniques for in vivo labeled leukocyte imaging have been developed. However, these techniques are not at present in widespread use [25].

Gallium Scan

Gallium is not frequently used in work-up of diabetic pedal osteomyelitis, but can be a useful alternative for assessment of pedal infection when there are abnormal radiographic findings on a foot radiograph and a labeled leukocyte scan or MRI is not available. Gallium-67 citrate localizes in areas of infection. If the gallium scan is normal, osteomyelitis can be excluded. By itself, gallium is not very specific for the diagnosis of osteomyelitis, because gallium accumulates not only at sites of bone infection but also at sites of soft tissue infection and at sites of increased bone remodeling, as seen in trauma [35]. Gallium scan images frequently lack spatial resolution, which precludes separation of bone from soft tissue uptake [35] (Fig. 6.8). If there is any bony abnormality, then a bone scan should be obtained prior to obtaining the gallium scan, in order to improve the specificity of diagnosis. (The long half-life of gallium-67 makes it prudent to acquire the bone scan first.) In that case, if the gallium scan is positive, then the uptake on the bone scan can be used to account for the gallium uptake that is occurring due to bony remodeling [36]. The diagnosis of osteomyelitis is made when the gallium and

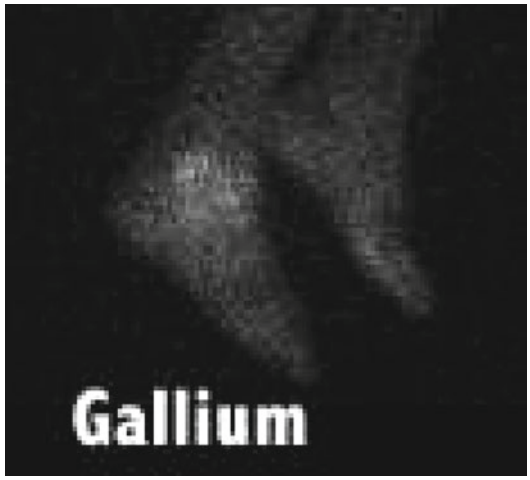

Fig. 6.8 Osteomyelitis of left ankle on gallium scan. The increased gallium activity in the distal tibia of a diabetic patient suggests osteomyelitis. However, the lack of resolution of the image precludes distinction of bone versus soft tissue inflammation

Table 6.3 Criteria for diagnosis of osteomyelitis using combined bone and gallium examinations [35]

Gallium uptake exceeds bone scan uptake
Gallium and bone scan uptake are spatially incongruent

bone scan are incongruent, as summarized in Table 6.3.

Schauwecker showed the sensitivity and specificity of this technique to be 81% and 69%, respectively [23]. However, the author also observed that more than half of the combined bone and gallium examinations were equivocal. This technique, therefore, is only helpful when the study is positive or negative. Although the relatively high number of equivocal examinations makes this modality less advantageous, gallium scan remains a useful alternative if labeled leukocyte scan or MRI is not available.

FDG PET Scan

Flourine-18 labeled fluorodeoxyglucose (FDG) imaging using positron emission tomography (PET) has become an important technique for oncologic imaging and is in common clinical use for detection, staging, and monitoring response to therapy in lung cancer, breast cancer, lymphoma, and melanoma, among others [37]. However, FDG PET scans often also show increased activity in areas of inflammation or infection and the use of PET for these nonneoplastic applications is now being actively investigated [37]. At this early juncture, however, FDG PET examinations are not routinely reimbursed for applications related to infection.

FDG is a radiolabeled glucose analogue that is taken up by cells in proportion to their metabolic rate and number of glucose transporter proteins. Increased FDG uptake is seen in inflammation, due to increased expression of glucose transporters and increased affinity for the glucose analogue by activated inflammatory cells. The fluorine-18 (^{18}F) radionuclide is produced in a particle accelerator known as a cyclotron and has a relatively short radioactive half-life. After intravenous injection of flourine-18 FDG, a patient is imaged 30–60 min later using a PET scanner. A routine examination includes images from the level of the skull base through the mid-thigh, though examinations spanning the skull to the feet can be performed. Areas of increased activity on the images reflect sites of increased glucose metabolism and may be described in terms of standardized uptake value (SUV). Many of the scanners currently being installed are PET-CT scanners, which incorporate both a PET scanner and a conventional CT scanner, In a PET-CT system, PET and conventional CT images are both obtained during the same examination and can be fused together into hybrid images, to aid in localization of areas of increased activity. This improved localization capability can be used, for example, to help distinguish between osteomyelitis and soft tissue infection [38].

FDG PET has shown promising initial results for imaging of infection, but remains an investigational technique. In general, sensitivity for infection tends to be relatively high and negative predictive value is very high, but false positives can occur because any area of increased metabolic activity—not just infection—will show increased radionuclide activity. Recent surgery can also result in false-positive increased activity [37]. Chacko et al. examined 167 PET scans in 175 anatomic sites and found an accuracy of

91.2% for chronic osteomyelitis [39]. Meller et al. prospectively compared FDG PET and labeled leucocytes and concluded that FDG was superior for the diagnosis of chronic osteomyelitis [40]. PET has also shown utility in evaluation of chronic osteomyelitis and infected prostheses [41]. In a meta-analysis by Termaat et al., FDG PET shows a pooled sensitivity of 96% and a specificity of 91% for the diagnosis of chronic osteomyelitis [42]. In a limited number of cases, correlative decreases in FDG uptake and inflammatory activity have been reported following antibiotic treatment [43], suggesting a potential role in tracking response to therapy, analogous to its current use in tumor treatment [37, 44]. A series of novel PET tracers are currently being evaluated for imaging of infection and inflammation [41]. Overall, FDG PET has shown good sensitivity for imaging of osteomyelitis [45], but is not yet reimbursed for this indication.

Specific data on the use of FDG PET for assessment of infection in the diabetic foot remains limited. Keider et al. examined 18 sites of infection in 14 patients and demonstrated that FDG PET could help to precisely localize infection and could distinguish between bone and soft tissue infection in the diabetic foot [38]. By contrast, in a study by Schwegler et al. that included seven diabetic patients with chronic foot ulcers and biopsy-proven osteomyelitis, FDG was positive in only two cases, while MRI was positive in six [46].

Compared with WBC scans, FDG PET offers shorter examination times and obviates the need for drawing WBCs from the patient for labeling. PET is less susceptible than WBC scans to false negatives resulting from decreased perfusion at the infection site. While PET and WBC scans are thought to be comparable in sensitivity in the peripheral skeleton (where there is usually a paucity of hematopoietic marrow to cause spurious WBC activity), PET is considered more effective than WBC scans for detection of central foci of infection/inflammation, because of physiologic uptake of WBCs by bone marrow in the axial skeleton [37]. A potential concern related to the use of PET in diabetic patients relates to the effect of chronic hyperglycemia on FDG uptake in metabolically active lesions [47].

Newer Radiopharmaceuticals

A number of new radiopharmaceuticals that may have application in the diagnosis of diabetic foot infection are being investigated, but have not entered routine clinical practice. These include radiolabeled antigranulocyte antibodies, immunoglobulins, and antibiotics.

Computed Tomography

Computed Tomography (CT) scans can show findings of osteomyelitis earlier than radiographs, but are not considered a front-line examination for the diagnosis of osteomyelitis, because they are less sensitive than MRI for soft tissue and osseous infection and also because, unlike MRI, they expose the patient to ionizing radiation.

CT scans use ionizing radiation to generate cross-sectional scans of the body. Tissues are displayed on a gray scale that reflects their relative X-ray attenuation, a quantity that is expressed in Hounsfield units (HU). For example, Hounsfield units typically measure −1,000 for air, 0 for water, ~ 40 for soft tissue, and ≥400 for bone. Most CT scans are now performed on multidetector scanners, which allow acquisition of thinner cross-sectional images and faster imaging times. When thin-section "volumetric" scans are acquired with a multidetector scanner, image sets acquired in one plane can be reformatted computationally into any desired imaging plane, after they have been acquired, e.g., images acquired axially can be reformatted into coronal or sagittal images. Image data can be postprocessed with different algorithms to highlight either bones or soft tissues. Independent of that postprocessing, images can also be displayed using "bone" or "soft" tissue windows. Image data can also be postprocessed to highlight anatomy in different ways, such as maximum intensity projection (MIP images) to produce a CT angiogram or volume rendering (VR) to create a 3D display of various tissues.

CT scans are often performed using intravenous iodinated contrast, in order to highlight different tissues, demonstrate characteristic enhancement patterns of certain structures,

outline cysts and fluid collections and distinguish them from solid masses, and depict vascular anatomy. In most cases, CT contrast administration is uneventful. However, some patients experience reactions after IV administration of iodinated contrast, with fatal anaphylactoid reactions in approximately 1 in 40,000 patients [48]. The risk of reaction is significantly reduced with low osmolar nonionic contrast, now in routine use at many institutions [49]. Use of nonioinic contrast also decreases the incidence of nausea, vomiting, hemodynamic instability, and discomfort or pain associated with contrast administration, effects that are relate to the osmolality of the contrast [49, 50]. In patients with a history of contrast allergy, nonionic contrast, together with oral methylprednisolone as a premedication, can be used prior to contrast administration. Patients with elevated creatinine (>1.5 mg/dL) and diabetes (especially insulin dependent diabetes) are at increased risk for contrast-induced renal failure due to acute tubular necrosis [51]. Contrast-induced nephropathy occurs with both ionic and nonionic contrast, although less frequently with nonionic forms. The overall incidence of contrast-induced renal failure is low (1–2% in patients with normal renal function) [49] and the effect is usually brief and self-limited. However, the rate is significantly higher in patients with renal failure (10% in patients with serum creatinine 1.3–1.9 mg/dL and up to 65% with levels >2 mg/dL) [49]. Moreover, contrast-induced renal insufficiency in a patient on the oral hyperglycemic agent dimethylbiguanide (Metformin) can result in fatal lactic acidosis, leading to the recommendation that Metformin should be withheld prior to and following contrast administration [49]. Intravenous hydration is used as a preventive measure in this setting; the use of diuretics may be deleterious [52].

Advantages of CT include high spatial resolution of CT images, superb depiction of bony detail and small calcifications, and the ability to image large areas of anatomy in a single, rapid scan. Disadvantages of CT include exposure to ionizing radiation and risks associated with contrast administration. Of note, the radiation dose from scanning extremities is significantly less than that associated with scans through the torso. Orthopedic hardware can cause "beam hardening" artifact that obscures surrounding anatomy, but, with newer generations of scanners, the effects are less pronounced than they have been in the past. Nonetheless, stents, dense prostheses, and large metallic constructs can pose problems for diagnostic imaging.

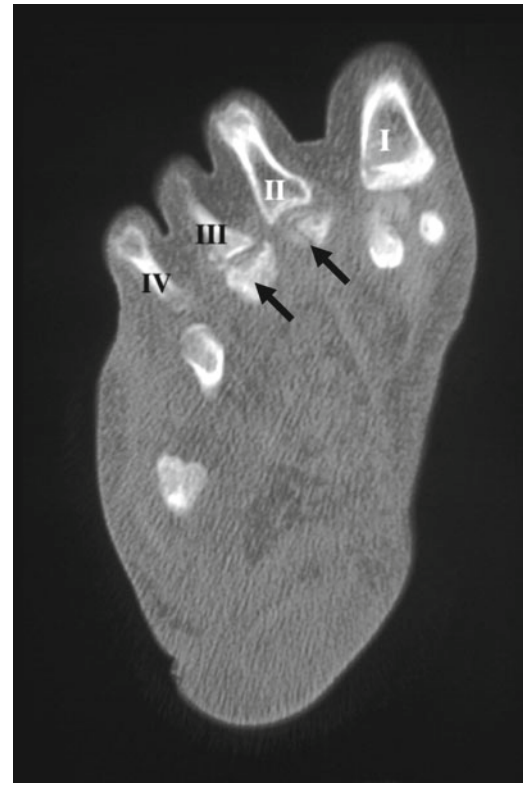

Fig. 6.9 Metatarsal osteonecrosis on CT. The second and third metatarsal heads are flattened. The radiolucencies beneath the deformed metatarsal heads represent subchondral fractures (*arrows*). CT exquisitely demonstrates these cortical abnormalities

During early stages of acute osteomyelitis, changes may be difficult to detect on radiography, but can frequently be documented on CT. CT is superior to radiography in detection of cortical destruction (Fig. 6.9), periostitis, and soft tissue or intraosseous gas [53, 54]. CT can also demonstrate increased density of intraosseous medullary fat and blurring of soft tissue fat planes due to the presence of pus and edema [55, 56]. CT is extremely effective in demonstrating a

bony sequestrum when present in chronic osteomyelitis (a focus of necrotic bone insulated from viable bone by granulation tissue). The sequestrum appears as a dense bone spicule situated within the medullary cavity and surrounded by soft tissue density [7, 57]. CT scan is useful for detection of radiographically occult foreign bodies, even those that are not traditionally considered radio-opaque (e.g., wood). While CT scans performed with intravenous iodinated contrast material can demonstrate soft tissues abscesses and necrotic tissue as areas of nonenhancement imaging modalities that possess superior intrinsic soft tissue contrast resolution, MRI and ultrasound are better suited to imaging of abscess collections and, when necessary, can be performed in the absence of intravenous contrast. Thus, use of CT for detection of soft tissue abscess should be weighed against the risk of contrast-induced complications. Overall, the data on sensitivity or specificity of CT for diagnosis of diabetic pedal osteomyelitis is scant. In light of concerns regarding risks of ionizing radiation, allergic reaction to contrast, and, in particular, contrast-induced nephropathy, there appears to be little enthusiasm for using CT as a routine diagnostic test for osteomyelitis.

Ultrasound

Gray-scale ultrasound has very limited application in imaging of bone and bone infection, because of the acoustic shadowing caused by cortical bone, though ultrasound has been used to image soft tissue infection and subperiosteal abscesses and can be used to guide aspiration of soft tissue infection. (Duplex Doppler ultrasound imaging of vasculature in the diabetic foot is discussed separately below.)

Ultrasound images are produced using an ultrasound transducer to transmit and receive ultrasonic waves of given frequencies, by holding the transducer against a patient's skin [58]. The amplitude of the sound that is reflected back (rather than transmitted forward) is translated into a gray-scale image of the underlying anatomy. Areas of interest are described based on their resultant echogenicity. Areas that transmit ultrasound waves with negligible reflectance, such as simple fluid, appear uniformly dark and are termed anechoic; areas that are highly reflective of sound waves, such as cortical bone, appear bright and are termed hyperechoic. Different tissues, such as muscles, tendons, and nerves, when normal, have characteristic reflectance patterns. Diagnostic ultrasonography of the foot is performed using a high-frequency transducer, often in conjunction with a stand-off pad.

Ultrasound has many advantages for imaging the diabetic patient. Ultrasound examinations do not involve ionizing radiation, entail minimal patient discomfort, and can often be performed in small children without the use of sedation. Ultrasound can be performed in patients who might have contraindications to MRI and can often yield diagnostic examination in cases where orthopedic hardware might preclude successful imaging by MRI or CT. Ultrasound equipment is relatively low cost, easily transportable, and is more widely available than MRI in many countries. Unlike many other imaging modalities, ultrasound readily provides real-time imaging and therefore can be used to assess motion and to guide aspirations, biopsies, and therapeutic injections. The major—and important—disadvantage of ultrasound is that it requires a high level of operator and interpreter expertise.

Ultrasound is well-suited for evaluation of superficial soft tissues and for guiding aspiration and drainage of intra- or extra-articular fluid collections. Abscesses are seen as hypoechoic collections with increased through transmission (i.e., the tissue deep to the abscess appears more echogenic than expected, because the sound waves are attenuated to a lesser degree by the fluid in the abscess than by the soft tissue surrounding the abscess) (Fig. 6.10). However, an abscess may be difficult to identify on ultrasound when its contents become proteinaceous, because it can then become isoechoic to the surrounding tissues and may fail to demonstrate enhanced signal in the tissues deep to the abscess. Similarly, joint effusions are often visible as hypoechoic on ultrasound, but may be less evident when their contents are complex. Even when sonography

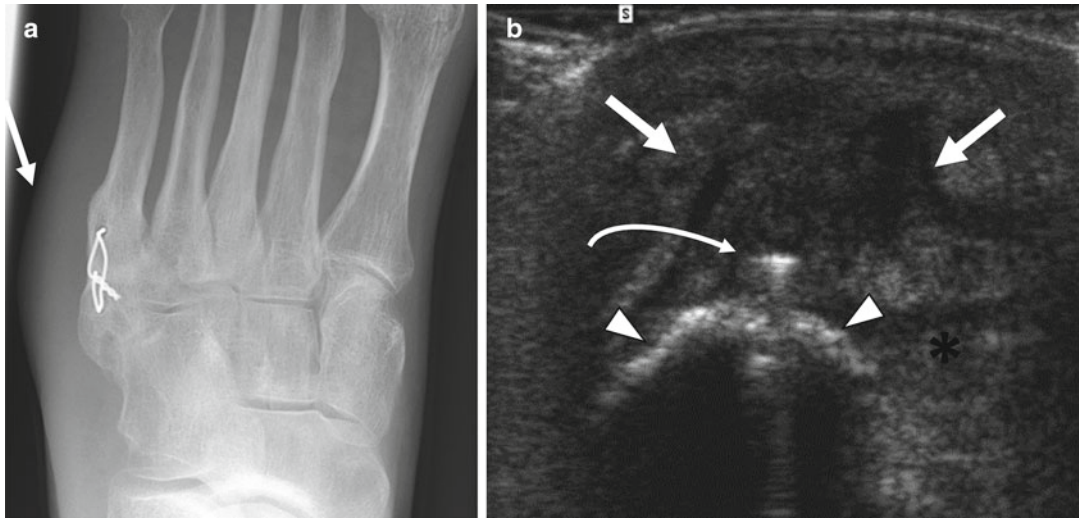

Fig. 6.10 Soft tissue abscess on ultrasound. (**a**) AP radiograph of the foot shows soft tissue swelling adjacent to the fifth metatarsal (*arrow*), but does not distinguish between generalized soft tissue swelling and detection of a focal abscess. (**b**) Gray-scale ultrasound image obtained in cross-section to the base of the fifth metatarsal shows a complex fluid collection in the overlying soft tissues (*arrows*), consistent with an abscess. Simple fluid appears anechoic (*dark*), but more complex components are similar in echogenicity to—and harder to distinguish from—surrounding tissues. The bright, hyperechoic curvilinear line is the cortex of the bone (*arrowheads*). The dark, anechoic area below the cortex is caused by acoustic shadowing from the cortex and (routinely) precludes ultrasound evaluation of the medullary cavity. The small bright area immediately above the cortex (*curved arrow*) represents an orthopedic wire. The bright, hyperechoic area next to the bone (*asterisk*) represents enhanced-through transmission, a sign that the tissue above it has fluid content

demonstrates a fluid collection, the presence or absence of infection within the fluid cannot be established by imaging. Thus, ultrasound is often employed for guiding aspiration of the suspect fluid collection.

Ultrasound is not very useful for direct evaluation of osteomyelitis, particularly early osteomyelitis, because cortical bone causes acoustic shadowing that obscures the underlying bone [59] (Fig. 6.10). In children, the use of ultrasound to demonstrate subperiosteal abscesses has been described [60, 61]. Subperiosteal abscess is a feature of osteomyelitis in children, but not adults, because, in children, the periosteum is more loosely adherent to the bone and, therefore, more easily displaced by pus. Subperiosteal abscess appears as an anechoic or moderately echoic zone >2 mm thick, adjacent to the bone and can be detected prior to changes on plain radiographs [62, 63]. Care must be taken not to mistake soft tissue abscess or soft tissue inflammatory changes adjacent to bone for subperiosteal abscess [64]. Power Doppler sonography can be used to demonstrate hyperemia surrounding a subperiosteal abscess, though it may not be positive in the early days of abscess formation [65]. Other signs associated with osteomyelitis that may be apparent at ultrasound include: fistulous communication between a subperiosteal abscess and the skin surface, swelling and edema in muscles immediately overlying the infected bone, and, in advanced cases, frank discontinuity of cortex [59, 66, 67]. Ultrasound can be very useful for detection of foreign bodies [68] (Fig. 6.11). Using ultrasound, an in vivo study of 50 patients with suspected nonradiopaque foreign bodies yielded a sensitivity of 95% and specificity of 89% for foreign body detection [69].

Because it can readily demonstrate musculoskeletal soft tissue structures and allows for accurate measurement, ultrasound has been used in a number of studies to identify correlates for degradation in biomechanical function in the diabetic foot. For example, D'Ambrogi et al. measured

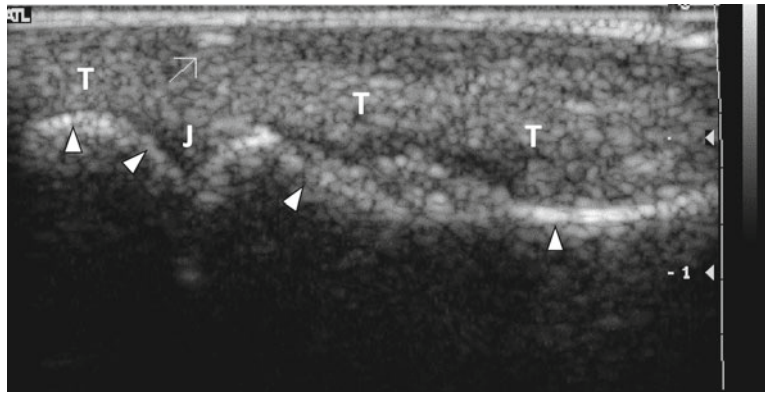

Fig. 6.11 Foreign body on ultrasound. Ultrasound image along longitudinal axis of a digit shows a small hyperechoic line (*arrow*) representing a small 12-mm foreign body. Thicker hyperechoic lines (*arrowheads*) represent the bony cortex, which obscures the underlying medullary cavity. *T* tendon, *J* joint space

the thickness of the Achilles tendon and plantar fascia in 61 diabetic patients (27 without neuropathy; 34 without) and 21 healthy volunteers and found significant thickening of the plantar fascia and Achilles tendon in the diabetic patients [70]. The abnormalities were more pronounced in neuropathic patients. Hsu and Wang et al. used ultrasound to compare the heel-pad mechanical properties in Type II diabetes patients with and without forefoot ulceration against healthy controls and found higher energy dissipation ratios when exposed to a load that simulated peak standing in-shoe plantar pressures within the heel pad of patients with Type II diabetes. They speculated that this could increase risk for developing foot ulceration [71].

Magnetic Resonance Imaging

Technique

Magnetic resonance imaging (MRI) is a primary modality for assessment of bone and soft tissue infection in the diabetic foot. Because it provides high intrinsic soft tissue contrast, MRI exquisitely depicts the full spectrum of soft tissues and can demonstrate radiographically occult bone marrow edema, without the use of intravenous contrast. Advantages of MRI over scintigraphy are precise anatomic definition and improved lesion characterization, lack of ionizing radiation, and shorter overall examination times. Because of its high sensitivity for abnormal bone and soft tissue edema and high negative predictive value, MRI can readily detect and delineate an infection's anatomic location and extent of an infection and can exclude infection when it is absent, making it a useful aid for surgical planning [9] (Table 6.4). Because of high sensitivity to marrow and soft tissue edema on MRI, however, it can sometimes be difficult to distinguish osteomyelitis and soft tissue infection from other causes of edema, such as fracture, early osteonecrosis, and reactive edema around an infection site. Postoperative changes can also cause marrow and soft tissue edema and can be impossible to distinguish from edema due to infection. MRI can be limited by artifact related to metallic hardware that can obscure the surrounding tissues. While patients with orthopedic hardware can usually be imaged, assessment of the area immediately surrounding metallic hardware is frequently limited by distortion of the local magnetic field. The extent of metal susceptibility artifact varies with the size and type of metal and can be minimized using certain imaging sequences (e.g., high-resolution

Table 6.4 Indications for MRI in detection of infection

Characterize soft tissue abnormalities
Exclude osteomyelitis
Preoperative assessment

fast or turbo spin echo sequences). Susceptibility artifact is generally more pronounced with stainless steel and less pronounced with titanium. Some, but not all, external fixation devices are MR-compatible. Some are ferromagnetic or paramagnetic and might displace in the magnetic field, so external fixation constructs must be tested for magnetic susceptibility prior to imaging. Moreover, any metal implant can result in local tissue heating, so patients with metal implants must be able to sense and communicate discomfort to the MR technologist at the time of imaging. MRI is contraindicated in patients who have pacemakers and other electronic implants, ferromagnetic cranial aneurysm clips, and intra-ocular metal. Some MRI-compatible versions of spinal stimulators and pacemakers have recently been developed, but these are not yet in common use. Most claustrophobic patients can be imaged with sedation or with the use of an open architecture magnet. The current generation of MRI machines, even when not formally described as "open" magnets, are built with shorter, wider bores ("tubes") and are often well-tolerated. Weight limitations for obese patients currently range from 300 to 450 pounds, depending on the magnet.

MRI scanners produce images using a strong magnetic field and radiofrequency (RF) waves. The magnetic field creates an equilibrium state for the atoms in the body, the RF wave perturbs the atoms, and the scanner then records how different atoms respond. Clinical magnets range in field strength from 0.2 to 3 T: the higher the field strength, the higher the potential signal-to-noise and spatial resolution (anatomic detail) in the resultant images. A variety of open, wide-bore, short-bore, and dedicated extremity magnets are now available. In order to optimally detect the signal produced by tissues in response to the radiofrequency wave perturbation and to generate high-resolution images, local RF receiver coils ("coils") are employed. Thus, for imaging the foot, a small diameter tubular extremity or foot-and-ankle coil is placed around the extremity. A typical MRI examination lasts 30–60 min, during which time approximately 4–8 imaging sequences are acquired. A sequence is a set of images designed to highlight specific tissue features and can be obtained in axial, coronal, sagittal, or any desired orientation. Some newer systems can obtain a 3D sequence that can then be reformatted into any plane. Imaging sequences are described in terms of the length of their TR (time-to-repetition) and TE (time-to-echo) times and in terms of any special radiofrequency pulses they employ (e.g., fat saturation or inversion recovery pulses). Commonly used imaging sequences are reviewed in Table 6.5. Anatomic and pathologic structures are described in terms of their signal intensity on a specific imaging sequence, often in relation to muscle. For example, fat and fatty marrow appear bright on T1-weighted images and are described as hyperintense or high signal intensity on T1-weighted images. They are low signal on fat-saturated T2-weighted and STIR sequences and are described as hypointense or low signal intensity. By contrast, simple fluid or edema is hypointense on T1-weighted images and hyperintense on T2-weighted, fat-saturated T2-weighted, and STIR sequences. Because gadolinium contrast and fat are both bright on T1-weighted images, contrast-enhanced images are often obtained using fat saturation techniques, so that fat appears darker and gadolinium contrast is bright. This is particular useful in the foot, where fatty marrow predominates. Optimal images are acquired by maximizing image signal-to-noise and using it to achieve high spatial resolution, based on appropriately small fields of view, thin slices, and smaller imaging voxel sizes. However, imaging at high spatial resolution requires longer imaging times.

Unlike CT, MRI provides high intrinsic soft tissue contrast, without the use of intravenous contrast agents. As a result, contrast is not required in order to detect changes of soft tissue infection or osteomyelitis—these processes appear as abnormal edema signal in the soft tissues and bones, respectively. However, contrast can play a role in imaging of infection in the diabetic foot by delineating soft tissue and intraosseous abscesses, highlighting fistulous tracts between ulcers and bone, and facilitating MR angiography. Gadolinium concentrates in areas of infectious or noninfectious inflammation

Table 6.5 MRI sequences—characteristics and applications

Sequence	Parameters	Use	Characteristics
T1 weighted (Fig. 6.10)	Short TE Short TR	Good for demonstrating anatomy	Normal fat and fatty marrow is bright or hyperintense on T1-weighted images
Proton density weighted	Short TE Long TR	Good for demonstrating anatomy	Similar to T1-weighted sequence, but fluid and muscle are not as dark or low signal
T2 weighted	Long TE Long TR	Fluid sensitive	Fluid and edema are bright or hyperintense on T2-weighted images, but may be hard to distinguish from fat, unless fat saturation is employed
Fat-saturated T2 weighted	Long TE Long TR ..... Fat saturation Pulse	Fluid sensitive (very)	Fluid and edema are bright or hyperintense; fat is dark or hypointense Very sensitive screen for fluid collections and for edema associated with infection or inflammation
STIR (Fig. 6.10)	Long TR Intermediate to long TE ..... Inversion recovery pulse	Fluid sensitive (very)	Normal fatty marrow is dark or low signal. Edema and fluid collections become bright or high signal Very sensitive screen for fluid collections and for edema associated with infection or inflammation, but anatomic detail is not well depicted
Fat-saturated proton density weighted	Short TE Long TR ..... Fat saturation Pulse	Fluid sensitive	Normal fatty marrow is dark or low signal. Edema and fluid collections become bright or high signal Can also screen for fluid and edema
T1 weighted with fat saturation ("fat sat") (Fig. 6.11)	Short TE Short TR ..... Fat saturation Pulse	Gadolinium contrast sensitive	Gadolinium contrast appears bright or high signal. Abscesses and proteinaceous or hemorrhagic fluid can also appear bright/high signal. Fat and simple fluid are dark or low signal Obtained both before and after IV contrast to detect contrast enhancement. Pre- and postcontrast sequences can be compared visually or computationally subtracted to demonstrate enhancing areas. Inhomogeneous fat suppression can occur When used without contrast

and produces hyperintense (bright) signal on T1-weighted images.

Most contrast agents employed for clinical MR imaging are based on the paramagnetic element gadolinium. Historically, gadolinium contrast has been better tolerated than the iodinated forms of contrast used for CT scans and catheter angiography, with lower risks of anaphylactic reactions and lower risk of nephrotoxicity. However, recently, gadolinium-based contrast media have been linked to the disease nephrogenic systemic fibrosis (NSF) in patients with severely impaired renal function [73, 74]. NSF, formerly known as nephrogenic fibrosing dermopathy, is a disfiguring and potentially disabling or fatal disorder, characterized by symmetric, coalescing, indurated skin plaques, that can also cause joint contractures and fibrosis in internal

organs. The link between intravenous gadolinium contrast and NSF is stronger for certain gadolinium formulations and seems to be dose-related [49]. Of note, follow-up dialysis after administration of gadolinium contrast does not appear to prevent NSF [74]. Due to concerns over NSF, the Federal Drug Administration (FDA) now recommends screening patients prior to administration of a gadolinium-based contrast agent to identify individuals with acute or severe chronic renal insufficiency. In our institution, this assessment is made in the MRI department, prior to contrast administration [75, 76].

Findings

On MR images, cellulitis appears as an ill-defined area in the subcutaneous fat that is of low signal on T1-weighted and high signal on STIR and T2-weighted sequences [16] (Fig. 6.2). It can be seen as both strand-like reticulate pattern of high T2 signal extending along septae between lobulaes of fat and of more confluent dense high T2 signal. However, this signal pattern is nonspecific and is common to both cellulitis and noncellulitic edema. Gadolinium administration may identify uncomplicated cellulitis, which typically shows uniform enhancement of subcutaneous edema [15].

Abscess presents as a focal lesion that is low signal on T1-weighted images and high signal on T2-weighted and STIR images. Without intravenous gadolinium, an abscess may not be distinguishable from dense soft tissue edema seen in severe cellulitis or from soft tissue phlegmon [72]. Following administration of intravenous gadolinium, an abscess demonstrates peripheral or rim enhancement, demarcating the fluid collection within (Fig. 6.12). The enhancing rim is believed to correspond to granulation tissue in the pseudocapsule. However, rim enhancement is a sensitive but nonspecific sign for abscess and can be seen in necrotic tumors, seromas, ruptured popliteal cysts, and hematomas [72]. Pus in the center of the abscess can have variable signal intensity, depending on its contents. Simple fluid will have low T1/high T2 signal, but abscesses often have high T1 signal content due to the presence of proteinaceous material within the fluid. Like proteinaceous fluid, hemorrhage can also appear high signal on T1-weighted images. Because this high T1 signal intensity appearance could be mistaken for gadolinium enhancement, comparison of pre- and postcontrast images becomes essential.

The diagnosis of septic arthritis is generally made clinically and confirmed by percutaneous joint aspiration or surgery [15]. The MR appearance of septic arthritis consists of joint effusion, often with synovial thickening, intra-articular debris, and surrounding reactive marrow and soft tissue edema. Following administration of intravenous gadolinium, there is intense synovial enhancement. Periarticular reactive marrow edema may demonstrate gadolinium enhancement even in the absence of osteomyelitis [15]. This constellation of findings is suggestive, but not specific for, infection and can also be seen in inflammatory conditions such as rheumatoid arthritis and seronegative arthropathies.

The primary MRI finding in osteomyelitis is abnormal marrow signal that enhances [72]. The abnormal marrow appears low signal (dark) on T1-weighted images and high signal (bright) on fluid-sensitive images such as fat-saturated T2-weighted and STIR images, typically with ill-defined margins (Fig. 6.1; Table 6.6). Changes in marrow signal intensity can be detected as early as 1–2 days after onset of infection [25, 77]. Following intravenous administration of gadolinium contrast, the abnormal marrow enhances and is seen as a bright area on the fat suppressed T1-weighted images. Secondary signs of osteomyelitis include cortical interruption, periostitis (seen as enhancement at the margins of the periosteum), and a cutaneous ulcer or sinus tract in contiguity with the abnormal marrow [15, 78]. Contrast does not identify new areas of signal abnormality compared with fat-saturated T2-weighted or STIR sequences [77]. Rather it helps demonstrate soft tissue and intraosseous abscesses and outline fistulous tracts between osteomyelitis and the skin [77]. It can also distinguish joint fluid from thickened synovium. Morrison et al. reported improved sensitivity and specificity for detection of osteomyelitis, using gadolinium contrast—88% sensitivity and 93%

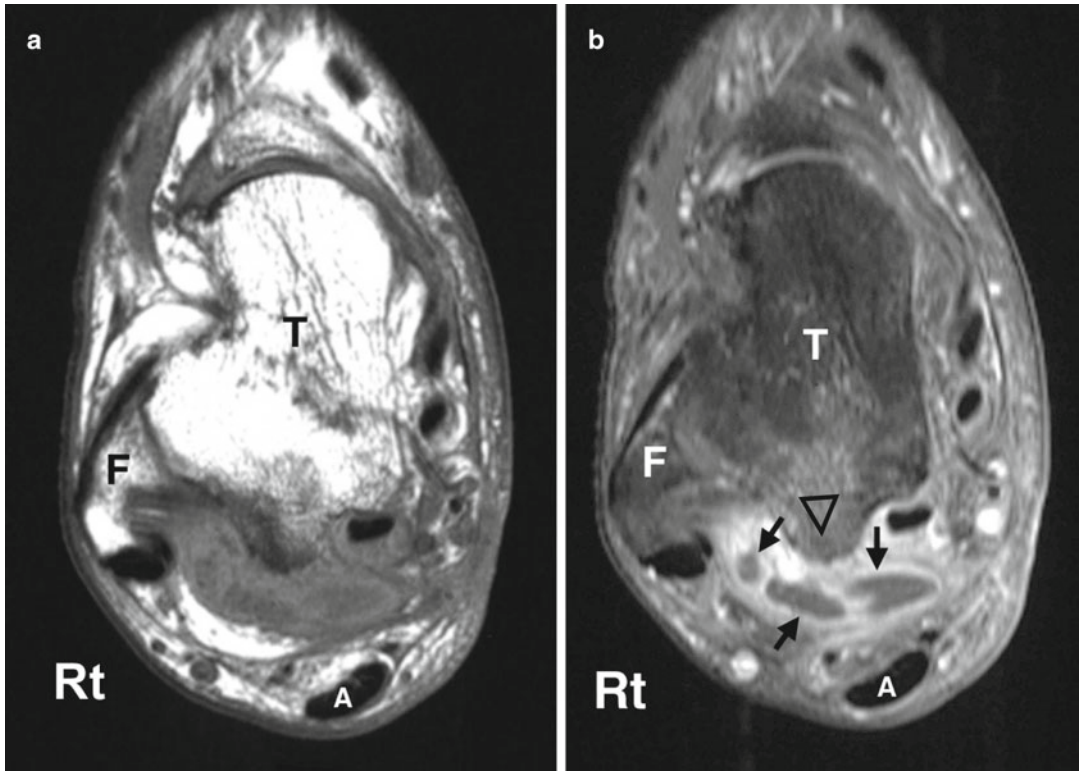

Fig. 6.12 Soft tissue abscess on MRI. Axial images of the ankle in a diabetic patient with ankle swelling. T1-weighted image (**a**) shows abnormal low signal posterior to the talus. Fat suppressed T1-weighted image (**b**) was obtained after IV administration of gadolinium. Note the bright enhancing peripheral rim (*arrows*) surrounding the abscess. The rim is slightly thickened. Central nonenhancement confirms fluid content. Enhancement is also seen in the adjoining portion of the talus and the intervening talar cortex is thinned and irregular (*open arrowhead*). Because they abut the abscess, these findings in the bone are highly suggestive of osteomyelitis. *A* Achilles, *F* fibula, *T* talus

Table 6.6 MRI findings of osteomyelitis

Primary signs
Hyperintense (bright) marrow signal on STIR sequence
Hypointense (dark) marrow signal on T1-weighted sequence
Enhancing marrow on postcontrast T1-weighted sequence
Secondary MR signs
Periosteal reaction
Subperiosteal abscess
Periostitis (manifested by periosteal enhancement)
Cortical destruction
Ulcer
Sinus tract

specificity for contrast-enhanced studies versus 79% sensitivity and 53% specificity for noncontrast-enhanced images [72]. Sensitivity and specificity of various secondary signs for identifying osteomyelitis were: sinus tracts (32%/85%), cellulitis (84%/30%), soft tissue abscess (26%/74%), ulcers (41%/81%), cortical tract or disruption (86%/78%) [78]. A negative MRI effectively excludes osteomyelitis (Fig. 6.3) [79].

The sensitivity and specificity of MRI for detection of osteomyelitis compiled from five studies is 96% and 87%, respectively [80–84].

Sensitivities and specificities for detection of osteomyelitis in diabetics are lower, respectively, 82% and 80%, in large part due to neuroarthopathic changes [72, 85]. Ahmadi et al. identified features that can help to distinguish between osteomyelitis and neuropathic arthropathy. They examined 128 neuropathic joints in 63 patients and concluded that features more indicative of infection were sinus tract, replacement of soft tissue fat, fluid collection, or extensive marrow abnormality, while features indicative of neuroarthropathy without infection were a thin rim of peripheral enhancement around an effusion, the presence of subchondral cysts, or the presence of intra-articular loose bodies.

Because of its high negative predictive value, MRI can facilitate accurate depiction of the maximum possible extent of marrow involvement by osteomyelitis. As such, MRI can help for planning of foot-sparing surgical procedures [72]. Marrow involvement is well-demonstrated on fluid-sensitive images, such as fat-saturated T2-weighted or STIR sequences.

Its advantages notwithstanding, MRI has several important limitations. MRI of the infected diabetic foot yields a significant number of false-positive diagnoses. The kind of abnormal marrow signal associated with osteomyelitis can also be seen with neuroarthropathy, including silent bone stress injuries associated with diabetic neuroarthropathy, bone contusions, fractures (Figs. 6.13 and 6.14), and, occasionally, osteonecrosis. The hyperemic phase of osteoarthropathy may display enhancing marrow edema indistinguishable from osteomyelitis. Intense soft tissue inflammation may also give rise to reactive edema in the adjoining bone, in the absence of osteomeylitis. False-negative contrast enhancement can occur in the setting of vascular insufficiency [86]. The utility of MR imaging for following response to treatment of osteomyelitis remains to be defined. Due to its high sensitivity for detection of soft tissue and marrow edema, MRI findings can be expected to lag behind the clinical response in treatment of soft tissue infection and osteomyelitis. As noted

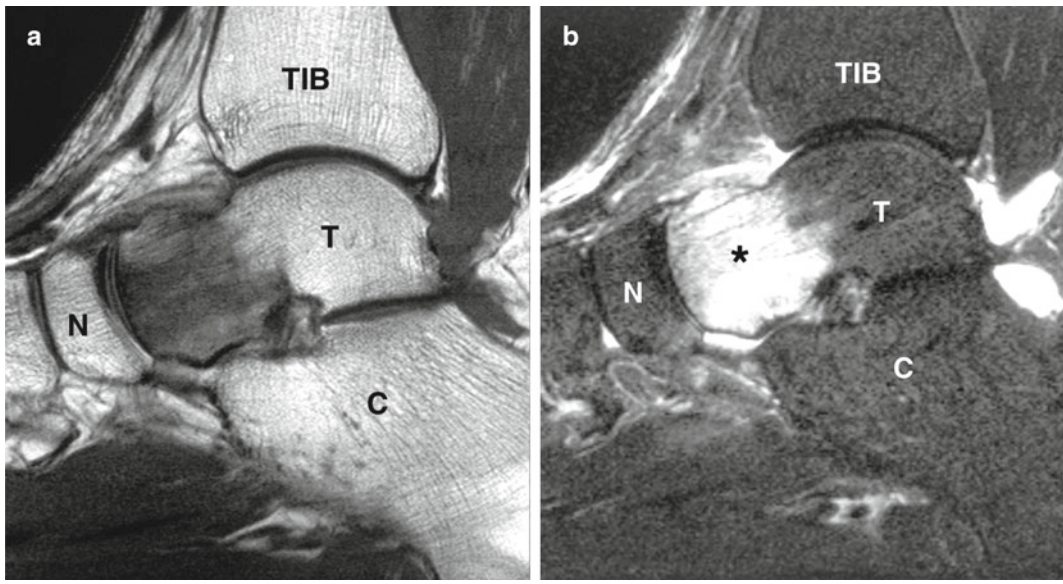

Fig. 6.13 Marrow edema on MRI. Sagittal images of the ankle show marrow edema (*asterisk*) which is (**a**) dark on T1-weighted image and (**b**) bright on STIR images. This marrow edema pattern is nonspecific and is similar to the marrow changes in osteomyelitis. However, this patient sustained trauma to the anterior talus and, here, the marrow edema represents a bone bruise. Specificity and accuracy can be improved by administration of gadolinium, as osteomyelitis frequently shows marrow enhancement. *C* calcaneus, *N* navicula, *T* talus, *TIB* tibia

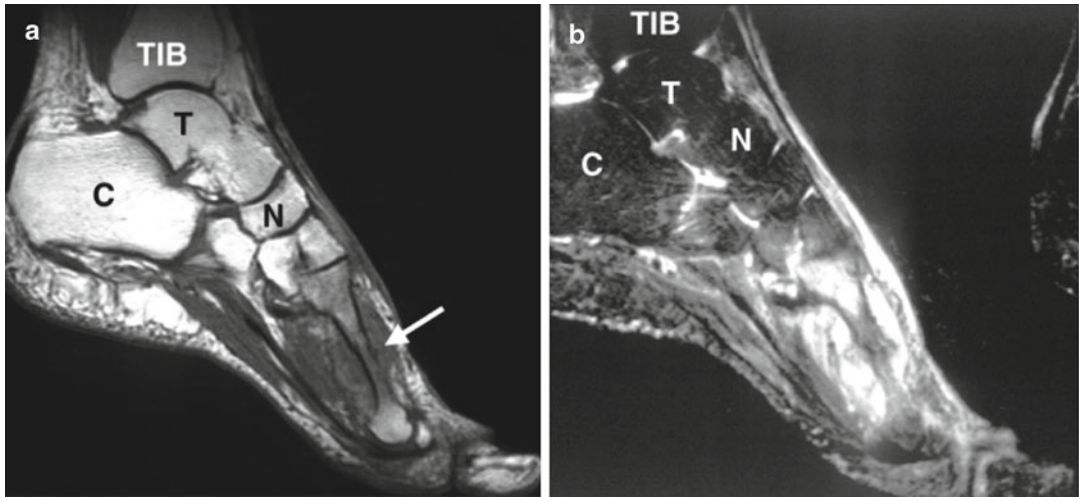

Fig. 6.14 Stress fracture on MRI. Sagittal T1-weighted (**a**) and STIR (**b**) MR images of the foot demonstrate cortical irregularity of the mid-diaphysis of the metatarsal bone (*arrow*). The marrow signal is abnormal, consistent with a marrow edema pattern: low signal on the T1-weighted image and high signal on the fluid-sensitive STIR image. The fracture line (*arrow*) remains dark on both sequences and is surrounded by bright edematous marrow on the STIR image. Marked soft tissue swelling surrounding the fracture is also better appreciated on the STIR images (**b**). *C* calcaneus, *N* navicular, *TIB* tibia, *T* talus

above, the use of gadolinium contrast in patients with severe renal failure is now a contraindication to gadolinium.

In addition to assessment of bone and soft tissue infection, there is great interest in the use of anatomic MRI [87–89], MR spectroscopy [90–92], and MR elastography [93] to identify early changes of structural and metabolic pathology in the diabetic foot.

Angiography

Angiography is indicated in diabetic patients with nonhealing ulcers or osteomyelitis who require mapping of vascular disease prior to endovascular or surgical treatment. Almost without exception, patients with nonhealing foot ulcers will have severe steno-occlusive disease involving all three runoff vessels of the calf (anterior tibial, posterior tibial, and peroneal arteries). In this patient population, 20% of peripheral bypass grafts will have to extend to a pedal artery. The distal anastamosis is either to the dorsalis pedis artery or to the proximal common plantar artery trunk [94]. Thus, detailed mapping of arterial disease from the abdominal aorta to the pedal vessels is necessary.

Several alternative—and, in some cases, complementary—techniques currently exist for mapping the vessels in the diabetic foot: conventional and digital subtraction angiography (DSA), MR angiography, CT angiography, and duplex Doppler ultrasound. These techniques are reviewed below. In general, vascular disease in diabetics tends to predilect the smaller caliber vessels of the distal lower extremity, which poses special challenges for imaging.

Catheter Angiography—Conventional and Digital Subtraction Angiography

Traditionally, vascular imaging has been performed using conventional angiography [95]. Conventional angiography is an invasive procedure, performed in the angiographic suite under fluoroscopic (real-time X-ray imaging) guidance. A thin, flexible catheter is inserted into the aorta or arteries, usually via a femoral artery approach. A relatively large bolus of iodinated contrast is injected into the intra-luminal catheter and rapid

sequence radiographs are exposed. Although examination of the abdominal aorta and iliac vessels can readily be performed with a multiside-hole catheter in the abdominal aorta, examination of the femoral, popliteal, tibioperoneal, and pedal arteries entails placement of a catheter in the ipsilateral external iliac artery. Selective catheter placement has the advantage of limiting contrast burden in a patient group predisposed to renal insufficiency.

Digital subtraction angiography (DSA) has replaced the older form of hardcopy, cut-film angiography in most institutions [49]. DSA is particularly advantageous for imaging diabetic arterial disease, because it is superior in terms of demonstrating small caliber distal vessels and uses less contrast to do so. In DSA, a set of images of the limb is obtained prior to administration of contrast (known as a "mask") and stored electronically. AP and lateral images are then obtained during administration of contrast, along the length of the vessels of interest, including one perpendicular to the interosseous membrane, that separates out the anterior tibial and peroneal vessels. Pre- and postcontrast image sets are subsequently subtracted by the computer to generate a final DSA image set that shows the intra-arterial contrast map. (Fig. 6.15). Using DSA, the interventionalist can perform rapid road-mapping of the vasculature during a procedure, without having to wait for hardcopy films to be developed. Nonionic iso-osmolar contrast agents, although more expensive, are typically used because they are associated with less pain and a lower risk of contrast-induced nephropathy, a risk that is higher in diabetic patients [96]. Newer high-resolution flat panel image intensifiers can cover larger fields of view and facilitate fewer injections and decreased radiation exposure. Portable and surgical suite DSA systems are available.

Conventional angiography, including DSA, remains the gold standard for arteriographic imaging. The major advantage of conventional angiography is that it provides access to perform not only diagnostic but also therapeutic, vascular procedures, including angioplasty, atherectomy, stenting, and thrombolysis. A well-timed study can provide very high spatial resolution images of small vessels. The major risks of the DSA angiography include radiation exposure, potential for bleeding, injury to the vessel wall, dislodgment of embolic material, and risk of renal failure or allergic reaction from the iodinated contrast. Injury to the femoral artery access site can be decreased with the use of lower profile catheters and sheaths and the use of ultrasound-guidance for placing the catheter [49]. Not infrequently, vascular disease and slow flow can disrupt the timing of the examination, with resultant failure to demonstrate the distal vessels. This is especially problematic when demonstration of distal vessels is the key to planning a bypass graft procedure. Good technique is a key for successful opacification of the distal tibial and pedal arteries.

There are several strategies for reducing contrast in exposure in patients with renal insufficiency: (1) if the femoral pulse is normal, a choice may be made to limit angiographic imaging to the extremity itself, and forgoing examination of the aortoiliac arteries; (2) the catheter can be advanced distally, into the distal superficial femoral or popliteal artery, for the injection, instead of performing the injection proximally, in the external iliac artery; (3) full strength contrast can be diluted with normal saline; (4) carbon dioxide (CO_2) can be used, instead of iodinated contrast for examination of the aorta and pelvis [49].

MR Angiography

More recently, MRI has come to play a role in the imaging of arterial disease, in the form of MR angiography (MRA). MRA has the benefit of providing detailed anatomic mapping of arterial disease while, at the same time, obviating the need for arterial catheter placement and associated complications. Contrast-enhanced MRA (CE-MRA) and noncontrast-enhanced time-of-flight (TOF) MRA are the most commonly used techniques for performing MRA of the lower extremity [97, 98] (Figs. 6.16 and 6.17). Phase-contrast MRA, an alternative noncontrast-enhanced MRA technique, has not been in common use, but is being currently being revisited and new noncontrast-enhanced techniques are also being developed. Gadolinium, the contrast

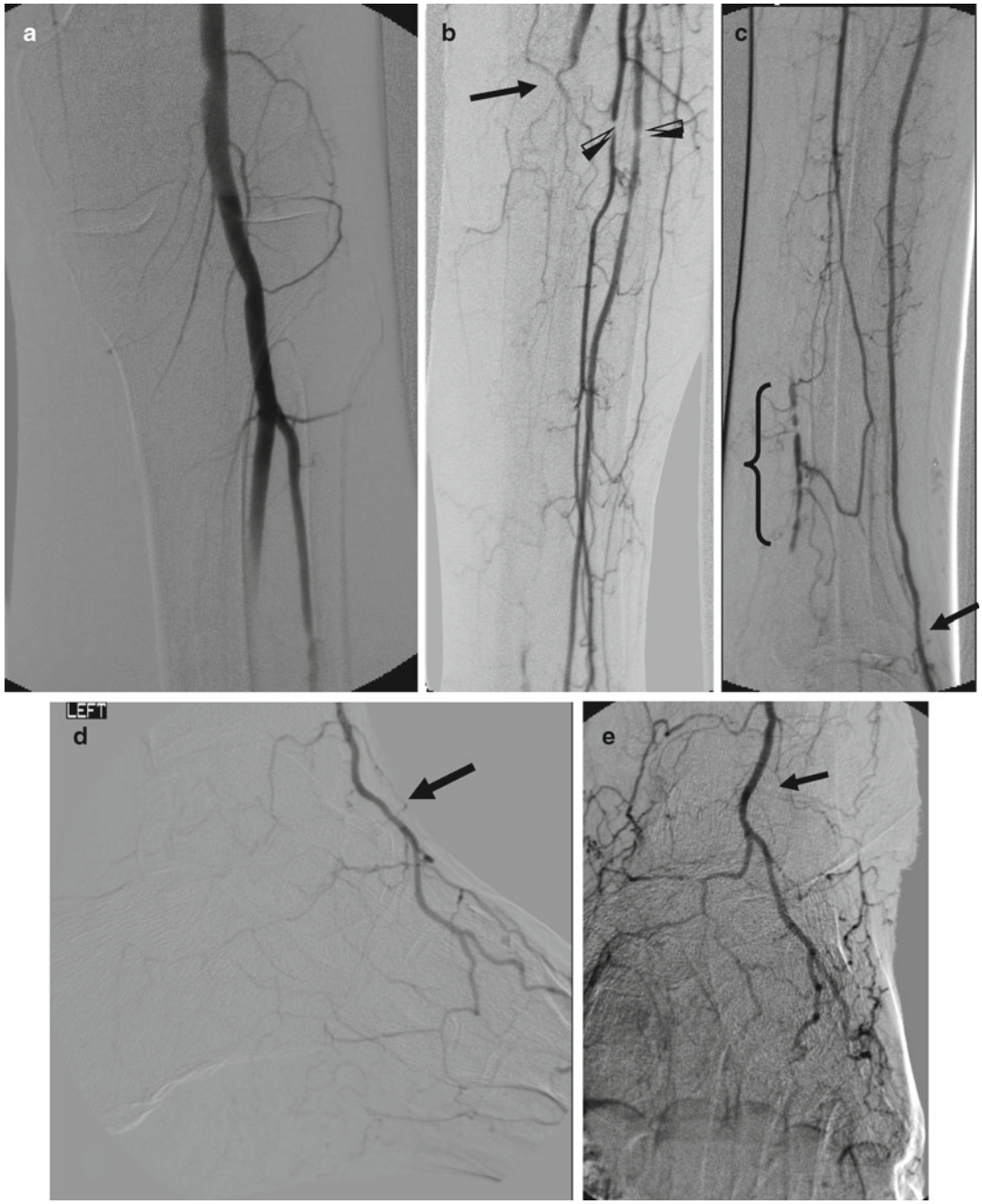

Fig. 6.15 Digital subtraction angiogram (DSA) of the lower extremity in 74-year-old diabetic man with non-healing heel ulcer. (**a**) Images demonstrate a patent popliteal artery, anterior tibial artery, and tibioperoneal trunk. (**b**) The posterior tibial artery is occluded (*arrow*) and there are stenoses in the proximal anterior tibial and peroneal arteries. (**c**) Just above the ankle, the left peroneal artery is occluded and there is reconstitution of a short diseased posterior tibial artery (*bracket*) from collateral vessels. The dorsalis pedis (DP) artery is patent (*arrow*). (**d**, **e**) Images in the foot show patent DP (*arrows*)

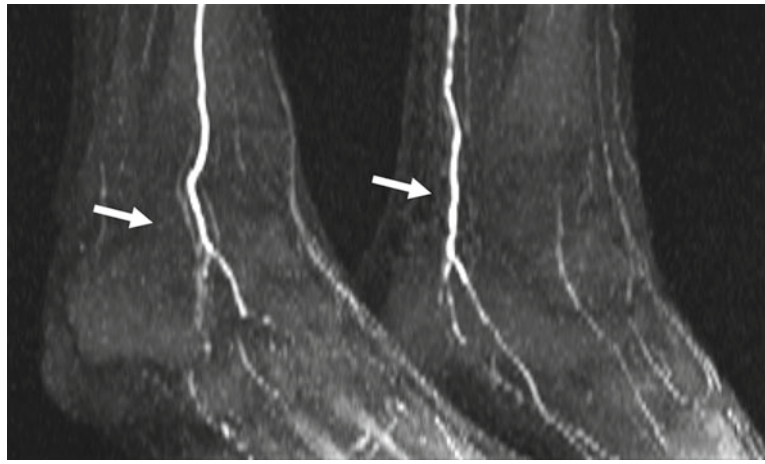

Fig. 6.16 Time-of-flight MR angiogram in the ankle and foot demonstrates single-vessel runoff, with patency of the posterior tibial artery and portions of the plantar arteries on both sides (*arrows*)

agent used in MRA, has traditionally been favored over the iodinated contrast used for catheter angiography, because of a lower incidence of allergic reaction and contrast-induced nephrotoxicity. However, new concerns regarding an association between gadolinium administration in patients with renal failure and development of a disease called NSF have arisen.

Time-of-flight MR angiography relies on a noncontrast-enhanced, flow-sensitive MR sequence. Computer postprocessing of the MR data generates coronal, sagittal, or oblique reconstructions that mimic the appearance of conventional angiograms. TOF MRA can be time consuming, requiring 1–2 h to cover the distance from the aortic bifurcation to the distal lower extremity. Cardiac gating of the MR images improves image quality, but lengthens examination time, especially when the patient has a cardiac arrhythmia or is on beta-blocker medication. TOF MRA images tend to exaggerate the degree of steno-occlusive disease and are prone to motion and metallic susceptibility artifact.

Gadolinium- or contrast-enhanced MRA (CE-MRA) relies on intravenous injection of a small volume of gadolinium contrast and rapid imaging that is timed to optimally follow the passage of the contrast bolus through the arteries. This technique has the advantage of short scan time, reduced motion, and reduced susceptibility artifacts. It is more accurate than TOF MRA examination in depicting the grade of steno-occlusive disease and offers higher resolution in the distal arteries of the lower extremity [99, 100]. CE-MRA uses a much smaller volume of contrast than conventional angiography and therefore generates a smaller osmotic load and subsequently a lower incidence of nephrotoxicity. However, visualization of the arteries can be limited by venous enhancement (Fig. 6.17) or by suboptimal arterial filling related to inaccurate timing of data acquisition. Use of new rapid image data-sampling techniques for CE-MRA, such as TRICKS (time-resolved imaging of contrast kinetics), can help improve imaging of arteries in the foot. Specifically, these kinds of sequences help address problems with proper timing of the contrast bolus and reduce "venous contamination" of images, while improving conspicuity of small distal vessels.

In general, MR angiography achieves sensitivities of 92–97% and specificities of 89–98% [101, 102] and compares favorably to conventional angiography. Both TOF and CE-MRA can reveal patent arteries not seen on conventional arteriograms [103, 104]. 3D CE-MRA is superior to 2D TOF MRA for detection and grading of peripheral arterial disease [104, 105]. Dorweiler et al. [106] examined the performance of pedal bypass grafts to foot vessels that were detected

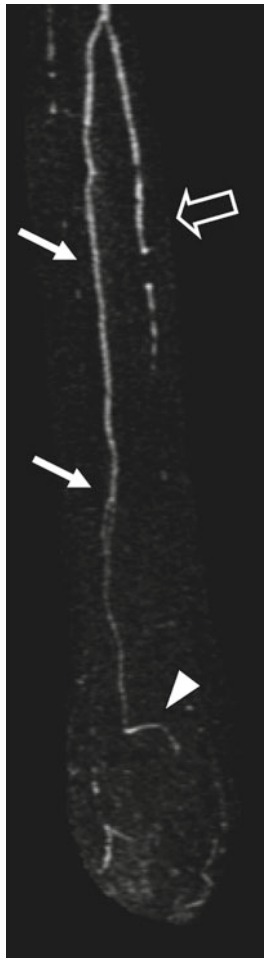

Fig. 6.17 Contrast-enhanced MRA for nonhealing ulcer. There is single-vessel runoff via the peroneal artery (*arrow*), to the level of the ankle joint, with reconstitution of an attenuated dorsalis pedis artery (*arrowhead*) via collaterals. The proximal posterior tibial artery demonstrates multiple stenoses and is occluded in the mid-calf (*open arrow*)

by MRA, but occult at conventional angiography, in 15 patients with diabetes mellitus and severe arterial occlusive disease [106]. During 22-month mean follow-up, there was one perioperative graft occlusion and one major amputation, resulting in a secondary patency rate of 93.1% and a limb salvage rate of 89.5% at 36 months. The appropriate clinical role of MRA in the management of arterial disease in the diabetic foot is debated [107].

Computed Tomographic Angiography

Lower extremity or peripheral computed tomographic angiography (CTA) is a relatively new technique for evaluation of the peripheral arterial tree. With the advent of multidetector CT (MDCT) in 1998, CT imaging became fast enough to allow scanning of inflow and runoff vessels in the entire lower extremity, with sufficient spatial resolution, in a single CT acquisition. The acquisition time for these images is on the order of less than 1 min [104]. The minimum number of channels required to generate a peripheral CT angiogram is provided by a 4-detector scanner, but later 16- and 64-detector machines are preferred, because they provide near-isotropic 3D image sets, allowing reformatting of high-quality images in any plane [104, 108]. Images are generated using standard intravenous CT contrast, injected into an antecubital vein via power injector. Sophisticated scanning protocols are employed to optimize opacification in the arteries of interest and the scanner table is moved during the scan to "chase" the contrast bolus. As with conventional angiography, optimal timing of the contrast bolus is affected by cardiac function and by delays due to arterial pathology in the infrarenal aorta and lower extremity arteries. Venous enhancement may contaminate arteriograms when there is significant arteriovenous shunting or when longer scan times are used, but, with good technique, this should rarely pose a diagnostic problem [104]. Artifactual narrowing or occlusion of the dorsalis pedis artery ("ballerina sign") can occur with excessive plantar flexion of the foot, as it can with other forms of angiographic imaging [109]. CTA involves a relatively high radiation dose [110] and requires large volumes of contrast (150–180 CC) per run.

Once the initial CT angiographic images are acquired (Fig. 6.18a), the data associated with those images can be postprocessed in order to generate clinically useful images (Fig. 6.18b–g), but this postprocessing requires a high level of expertise, in order to avoid introducing postprocessing artifacts that will degrade diagnostic accuracy. In some institutions, CT angiogram studies are postprocessed by specially trained

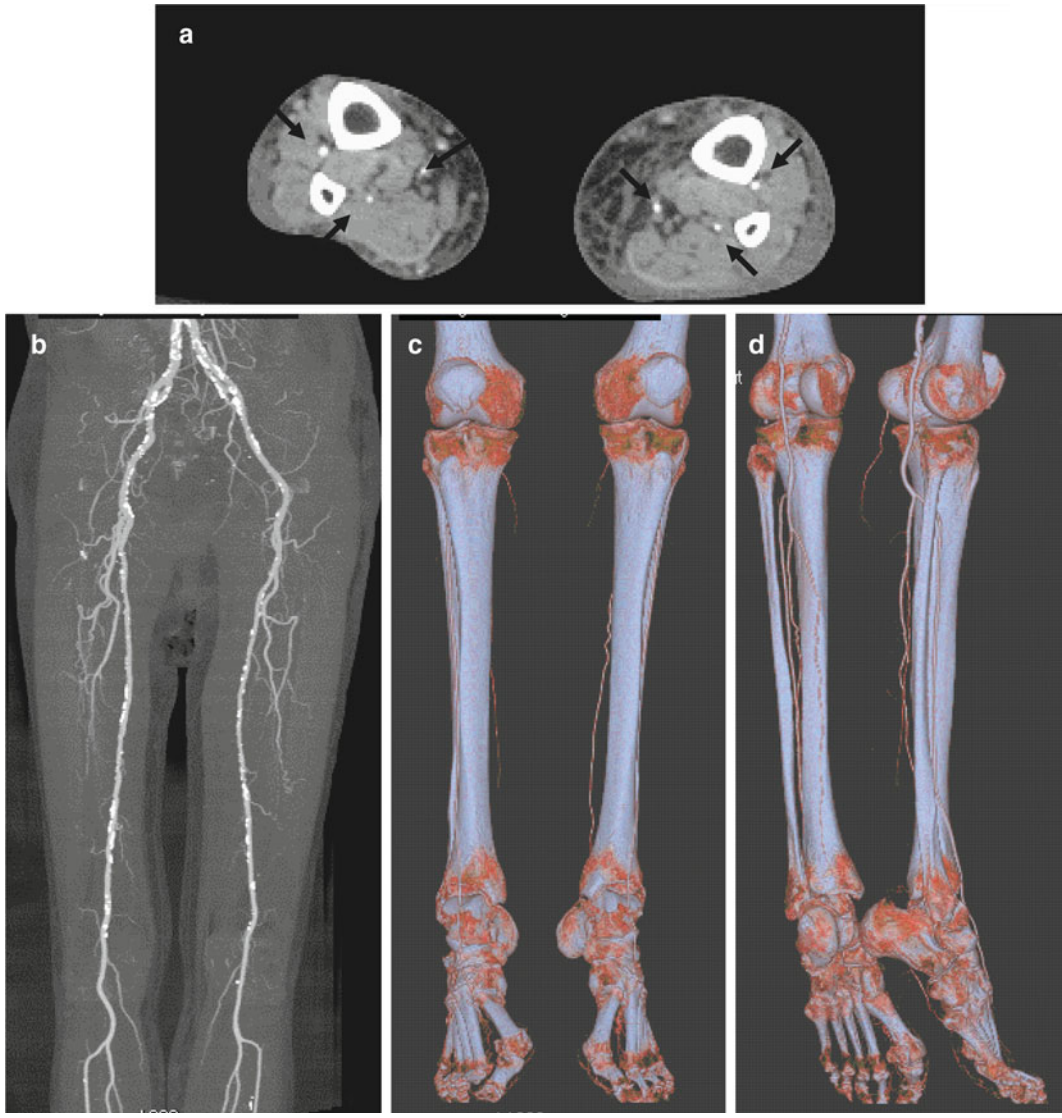

Fig. 6.18 CT angiogram with patent vessels in woman with concern for claudication. (**a**) Axial image of both lower extremities from a CT angiogram represents the source image for subsequent computer-generated postprocessed images. All three lower extremity runoff vessels are patent bilaterally, seen as small bright foci (*arrows*), due to administered contrast. (**b**) Maximum intensity projection (MIP) image was generated in the image processing lab from a stack of source images similar to (**a**) acquired through the lower body. The MIP mimics a conventional arteriographic display. Bilateral 3 vessel runoff (proximal portion) is well depicted. Based on the protocol, images can be extended distally. Scattered areas of higher density (whiter) seen along the vessels reflects the presence of calcified atherosclerotic plaque. (**c**) AP and (**d**) oblique volume rendered (VR) images display the vessels in relation to bony anatomy, based on Hounsfield unit density thresholds. (**e**–**g**) Curved planar reformatted images can be generated along the actual path of the vessel, in order to lay out the vessel in a single plane, respectively, depicting the anterior tibial, peroneal, and posterior tibial arteries

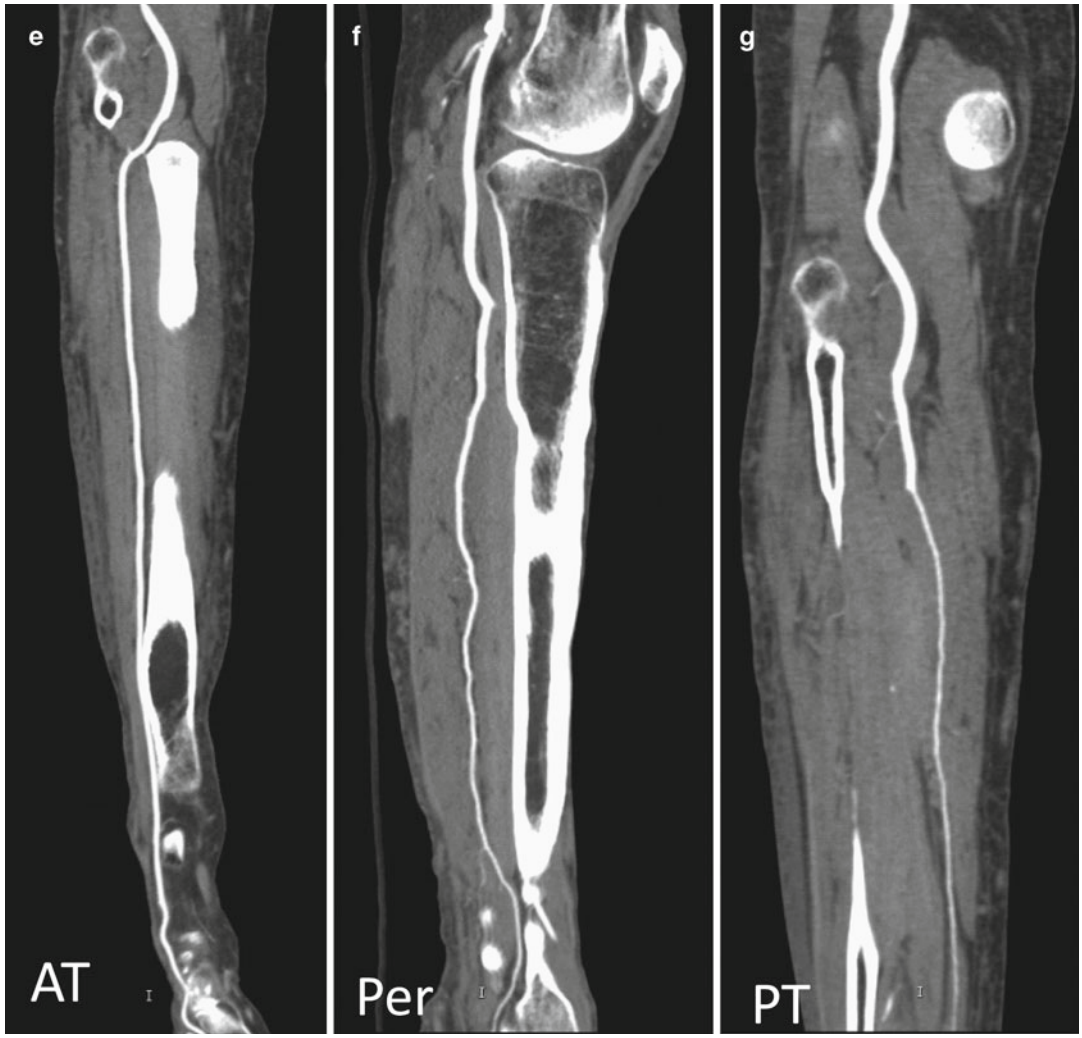

Fig. 6.18 (continued)

technologists in a dedicated image processing lab. Postprocessing techniques include MIP images, which mimic conventional angiography displays (Fig. 6.18b). These require subtraction of bone from the image, at which time there is a risk of inadvertently removing vessels adjacent to bone. Volume rendering (VR) represents a form of 3D surface display that does not rely on subtraction of bone from the image (Fig. 6.18c, d). In VR, however, vessels can be inadvertently removed by choice of VR parameters. In both MIP and VR techniques, stents and vessel calcifications can completely obscure the vessel lumen, making it difficult or impossible to assess flow in that segment—this can limit the utility of CTA in approximately 60% of patients with peripheral arterial occlusive disease [108]. In these cases, source images obtained perpendicular to the vessel can be useful. Curved planar reformations (CPRs), which are longitudinal cross sections generated along a predefined vascular center line, can be generated along the length of the vessel, regardless of its course (Fig. 6.18e–g), but they require manual or semiautomated tracing of the vessel center line. With CPRs, artifacts mimicking vessel stenosis or occlusion can occur when

the center line is not selected properly. When viewing CTA images, regardless of postprocessing technique, care must be taken not to overestimate stenosis or occlusion due to artifactual "blooming" of calcifications or stents on narrow viewing windows. A viewing window of at least 1,500 HU may be required [104]. Of note, when there is extensive vascular calcification in smaller crural or pedal arteries, it may be impossible to resolve the vessel lumen, notwithstanding proper window/level selection [104].

There is limited data available for assessment of the diagnostic accuracy of CTA in the evaluation of peripheral arterial occlusive disease. Wilmann et al. examined the use of submillimeter collimated 16-channel MDCT in 39 patients and found sensitivity of 96% and specificity of 97%, even in popliteo-crural branches, using an effective radiation dose that was lower than for conventional DSA [111]. To date, use of CTA for assessment of pedal arteries has not been reported. As suggested above, dense vascular calcification can potentially reduce diagnostic performance on MDCT [104, 112].

Doppler Ultrasound

In addition to its ability to provide gray-scale anatomic imaging, ultrasound can play an important role in depicting blood flow [113]. Three complementary techniques for blood flow imaging with ultrasound exist: (1) duplex Doppler ultrasound; (2) color flow imaging; and (3) power Doppler. These techniques are based on the Doppler effect: when a sound beam is reflected back off a moving object, the frequency of the sound beam is altered, increasing in frequency when the object (here, red blood cells) is moving toward the source of the sound beam, and decreasing when the object is moving away. The change in frequency is proportional to the velocity of the object and is greatest when the sound beam travels parallel to the vessel. Because Doppler measurements capture information about the velocity of blood flow, quantitative assessment of the severity of stenosis can be obtained, based on peak systolic and end-diastolic velocity measurements. Higher peak systolic measurements indicate more severe stenoses [114]. Using this technique, stenosis is graded as the ratio of peak systolic velocity of the target vessel divided by [the velocity in the adjacent nonstenosed vessel minus the peak systolic velocity ratio]. Findings are recorded on an anatomic diagram, creating a visual map of the vascular pathology. Doppler wave form analysis refers to depiction of the *pattern* of arterial blood flow, based on Doppler frequency shift. Patent arteries show a normal triphasic flow pattern. However, with increasing stenosis, the wave form flattens (Fig. 6.19). In duplex Doppler, the gray-scale ultrasound image of the vessel and the vascular waveform are depicted together (Fig. 6.20). Duplex Doppler ultrasound can be used to image arteries and veins, to assess the severity and extent of peripheral artery disease, and to identify pedal arteries for bypass. Color Doppler images depict the frequency shift data as a color spectrum that encodes both directional and velocity information. In color Doppler images, red and blue colors are superimposed on gray-scale anatomic images of vessels, to indicate, respectively, flow toward and away from the transducer. Color Doppler images are often used in conjunction with duplex Doppler to aid in visualizing vessels. Doppler measurements and resultant images may be degraded by aliasing artifacts, either when the sampling frequency is too low or the angle of incidence between the sound beam and the vessel are too low. The third technique, power Doppler, is more sensitive to blood flow than color Doppler, allowing it to show smaller vessels and slower flow rates. Power Doppler scans assign color to flow, independent of its direction. Because of its high sensitivity, power Doppler can demonstrate flow associated with inflammation and neovascularity, such as inflammation associated with soft tissue infection and in soft tissues adjacent to osteomyelitis. Power Doppler can also help to distinguish between phlegmon and abscess, based on the lack of flow within the center of an abscess. With power Doppler, artifactual "flow" can occur with movement of the transducer or body part and false-positive and -negative findings can occur if the ultrasound machine's settings (color gain) are not properly set.

Doppler

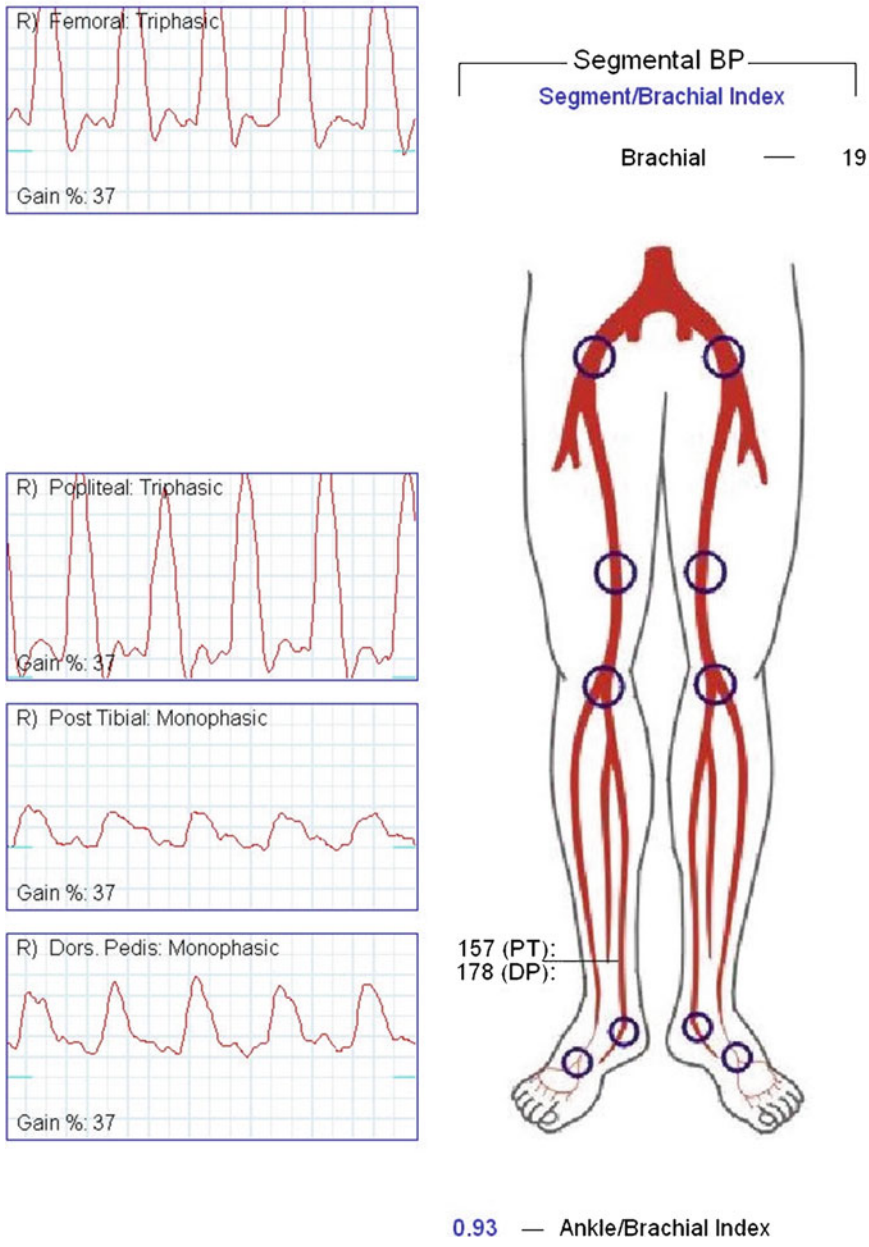

Fig. 6.19 Doppler wave from analysis in 62-year-old with right great toe ulcer and cellulitis. Arterial waveforms were evaluated using Doppler ultrasound at standardized sites along the ipsilateral lower extremity. While a normal triphasic wave pattern was observed in the femoral and popliteal vessels, a monophasic wave pattern was observed in the posterior tibial and dorsalis pedis vessels, indicating intervening stenosis

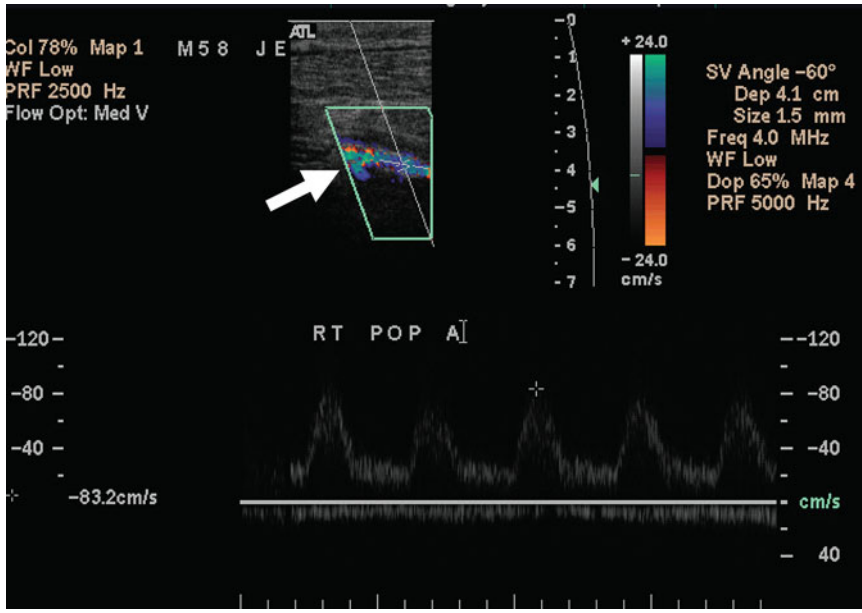

Fig. 6.20 Duplex Doppler examination at popliteal artery. The gray-scale ultrasound image of the popliteal artery (*thick arrow*) is used to position the cursor for the measurement. Here, Color Doppler is being superimposed on the vessel to help highlight the artery and arterial flow velocities. The popliteal artery waveform generated by the measurement is shown below. A cursor is placed at the height of the waveform peak (*thin arrow*) and yields a peak flow rate of 83 cm/s, with no evidence of stenosis. Duplex Doppler ultrasound can be used to generate data like this long the length of a vessel, in order to map the site, length, and severity of stenoses

Advantages of Doppler ultrasound are similar to those of ultrasound in general: the examination is noninvasive, avoids the hazards of an arterial puncture, does not require ionizing radiation or administration of nephrotoxic or allergenic contrast agents, and is generally well-tolerated by a variety of patients. Ultrasound is also less costly than preprocedure diagnostic angiography. Disadvantages of Doppler ultrasound include: operator dependence of the examination, relatively lengthy examination time, and limited ability to ensure that the entire area of interest has been imaged [104]. Mural calcification can cause acoustic shadowing and interfere with accurate measurement [115]. In practice, accurate Doppler measurements require a vascular laboratory with sufficient experience and attention to quality control. In the future, the use of ultrasound intravascular agents may contribute to improved imaging, but clinical utility of these techniques in the diabetic foot remains to be established [116].

Duplex ultrasound examination can be used for noninvasive preoperative planning of re-vascularization procedures in diabetic patients [115, 117]. Ultrasound can be used to map occlusions for length and stenosis, based on velocity profiles [115]. Though a complete discussion of the field is beyond the scope of this chapter, a number of studies have demonstrated the utility of duplex Doppler ultrasound in this setting. Doppler ultrasound interrogation can be performed with high degree of sensitivity and specificity in aortoiliac and femoropopliteal segments [117]. Duplex imaging of tibial vessels requires greater operator skill than imaging of larger, more proximal vessels, but can reliably identify stenosis and occluded segments and, in some cases, may be superior to angiography [118]. Hofmann et al. examined the use of preoperative high-frequency duplex scanning of potential pedal target vessels [119]. They studied 33 consecutive diabetic patients suffering from critical limb ischemia,

with indications of infra-popliteal occlusive disease, using a 13 MHz ultrasound probe, and attempted to identify the pedal target vessel best suited for surgery, based on inner diameter, degree of calcification, maximal systolic velocity, and resistive index. Results of Duplex scanning were compared with (1) results of selective digital subtraction arteriography (DSA) and contrast-enhanced MRA interpreted by two radiologists; (2) the site of distal anatamosis predicted by a vascular surgeon based on the MRA and DSA; (3) the definitive side of distal anastamosis; and (4) early postoperative results. They found that Duplex scanning depicted significantly more pedal vascular segments than selective DSA, with relatively high agreement between the duplex ultrasound prediction and the definitive site of anastamosis (kappa 0.82). Levy et al. examined 105 consecutive lesions angioplastied among 56 patients undergoing 60 endovascular procedures, including aortoiliac, infra-inguinal, and bypass graft lesions. Of these procedures, completely noninvasive evaluation was accomplished in 43 procedures (73%), either by means of duplex scanning ($n=11$, 18%) or by means of MRA ($n=32$, 53%) [120]. The findings at noninvasive examination were confirmed at intraoperative angiography and no additional lesions were identified. ABI and mean limb status category both showed significant improvement. The noninvasive approach was less expensive compared with preprocedural contrast angiography, with $551 saved for each duplex scanning case and $235 saved for each MRA case (not including the $144 cost of postprocedure short-stay unit time required for diagnostic arteriogram).

Angiography Summary

Multiple modalities are now available for angiographic imaging of the lower extremity in the diabetic patient. Catheter angiography, now primarily performed using DSA, is considered the gold standard, because it provides the highest potential spatial resolution, including, in particular, spatial detail in the smaller crural and pedal vessels. Catheter angiography carries risks associated with an invasive technique, but provides the opportunity to combine the diagnostic study with definitive treatment of certain kinds of arterial stenoses. MRA, CTA, and duplex Doppler ultrasound provide noninvasive alternatives for angiographic imaging and continue to improve their capacity to image subtle disease and small vessels. All types of angiographic imaging are reliant on achieving optimal technique in generating and postprocessing of images, in order to attain the highest level of diagnostic accuracy. While the MR contrast, gadolinium, has traditionally been favored over iodinated contrast agents for its low rate of allergic reaction and low incidence of nephrotoxicity, new concerns about the association of NSF with the use of certain gadolinium contrast agents in patients with renal insufficiency have limited its use in patients with renal failure.

Osteomyelitis Versus Neuroarthropathy

Differentiation between osteomyelitis and neuroarthropathy is often difficult. Certain neuroarthropathic changes resemble osteomyelitis. In order to better understand the similarities and differences, imaging characteristics of neuroarthropathy will be presented here. A more complete discussion of neuro-osteoarthopathic changes is provided in another chapter of this book.

Neuroarthropathy

Loss of both pain and proprioceptive sensation is believed to predispose to repetitive trauma, leading to diabetic neuroarthropathy [15]. Though potentially devastating, the incidence of neuropathic joints in the diabetic is surprisingly low, reported to be 0.1–0.5%. The joints of the forefoot and midfoot are commonly involved. The distribution of neuroarthropathy in diabetic patients is 24% in the inter-tarsal region, 30% in the tarsometatarsal region (Fig. 6.21), and 30% in the metatarsophalangeal joints. Abnormalities of the ankle (11%) and interphalangeal (4%) joints are less frequent [121].

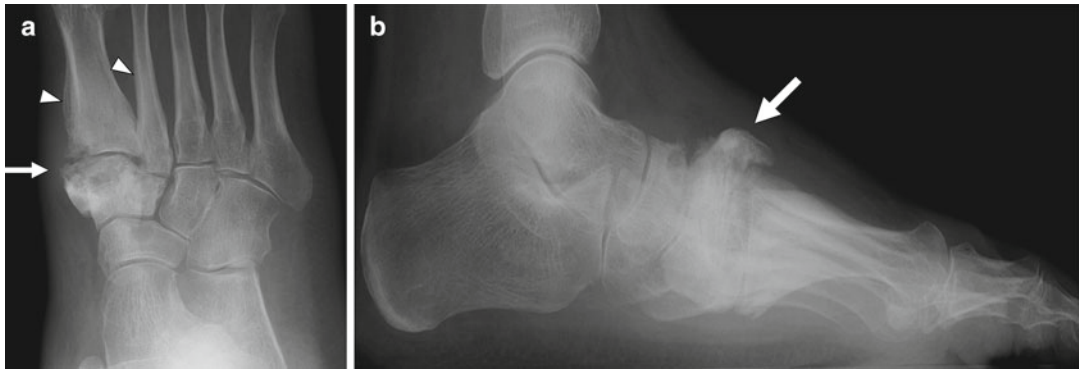

Fig. 6.21 Hypertrophic form of neuroarthropathy. (**a**) AP and (**b**) lateral radiographs show hypertrophic changes in the medial midfoot (*arrows*), centered about the tarsometatarsal joint. There is bony proliferative change, increased density and nonaggressive periosteal new bone formation (*arrowheads*) in the first and second metatarsal bones, and increased density in the corresponding cuneiforms. In its early phase, this form of neuroarthropathy may be confused with osteoarthritis. Note soft tissue swelling, with effacement of fat planes

Two classic forms of neuroarthropathy, atrophic and hypertrophic, have been described [122]. The atrophic form, representing the acute resorptive or hyperemic phase, is characterized by osseous resorption and osteopenia. This form frequently appears in the forefoot and the metatarsophalangeal joints, leading to partial or complete disappearance of the metatarsal heads and proximal phalanges. Osteolytic changes produce tapering or "pencil-pointing" of phalangeal and metatarsal shafts. Marrow changes in the atrophic or hyperemic form show hypointense T1 and hyperintense STIR and mimic the changes seen in osteomyelitis. The hypertrophic form, representing the healing or reparative phase, is characterized by sclerosis, osteophytosis, and radiographic appearance of extreme degenerative change (Fig. 6.21). In its early phase, the hypertrophic form of neuroarthropathy may be confused with osteoarthritis. Concurrent osseous fragmentation, subluxation, or dislocation predominates in the inter-tarsal and tarsometatarsal joints. Ruptured ligaments in the mid- and forefoot cause dorso-lateral displacement of the metatarsal bones in relation to the tarsal bones. This classic finding resembles an acute Lis-Franc fracture-dislocation (Fig. 6.22). Disruption of the talonavicular and calcaneocuboid joints causes collapse of the longitudinal arch, with subsequent plantar displacement of the talus. These changes produce the classic "rocker-bottom" deformity [123]. Recognition of this deformity is important because it creates new pressure points that lead to callus formation and ulceration (Fig. 6.23). Attempts to classify neuropathic joints into the two classic forms may be difficult, as a mixed pattern, composed of both forms, occurs in 40% of neuropathic joints [124].

Osteomyelitis Versus Neuroarthropathy

Other than the characteristic findings of diffuse dark marrow signal on T1-, STIR and T2-weighted MR images associated with hypertrophic neuroarthropathy (versus high T2 and STIR signal seen in osteomyelitis), there is no easy method of distinguishing between osteomyelitis and neuroarthropathy. Secondary findings such as involvement of the midfoot and multiple joints, absence of cortical destruction, presence of small cyst-like lesions, and distance between soft tissue infection and bone changes favor a diagnosis of neuroarthropathy (Table 6.7) [15]. By contrast, osteomyelitis favors the toes or metatarsal heads, and is associated with focal cortical lesions and close proximity to the ulcer.

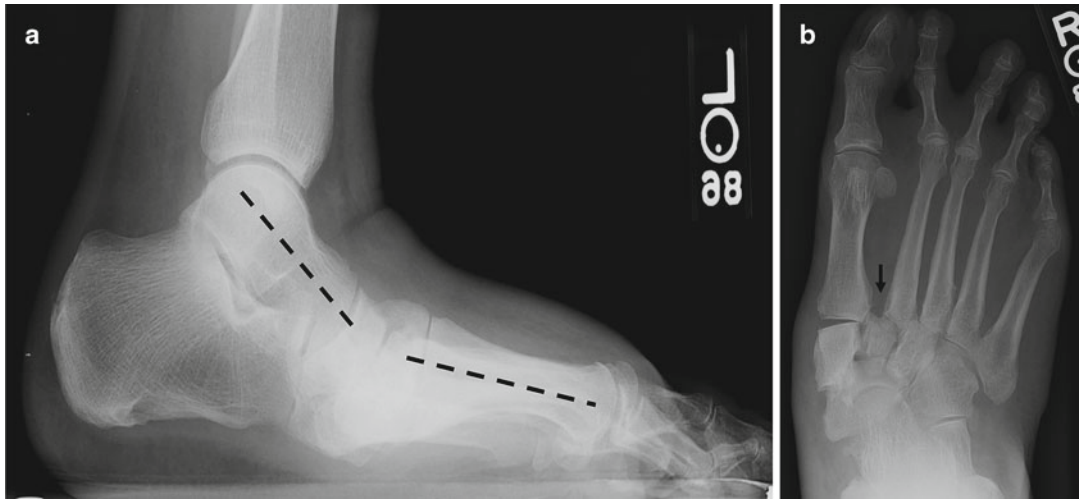

Fig. 6.22 Midfoot deformity related to neuroarthropathy. (**a**) Lateral radiograph demonstrates collapse of the usual longitudinal arch of the foot. Progression can result in extreme "rocker-bottom deformity." (**b**) AP view shows Lis-Franc malalignment (*arrow*) as well as disruption of the navicular-cuneiform articulations

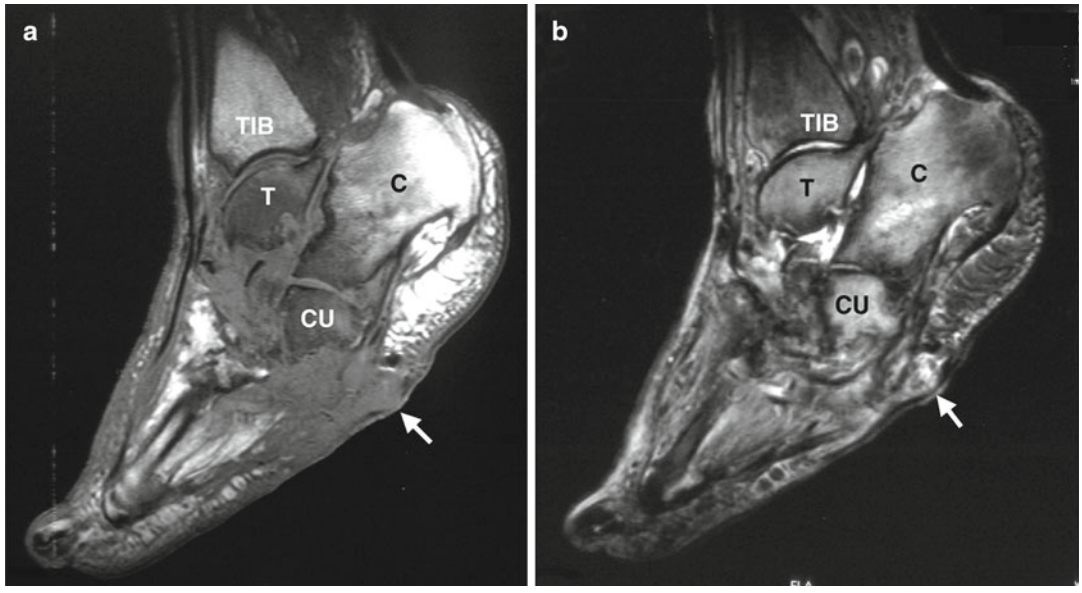

Fig. 6.23 Rocker-bottom deformity and ulceration at focus of high plantar pressure on MRI. (**a**) Sagittal T1-weighted and (**b**) STIR images show disruption of the talonavicular joint causing collapse of the longitudinal arch. These changes produce the classic "rocker-bottom" deformity. This deformity is important because it creates new pressure points that lead to callus and ulcer formation (*arrow*). The diffuse marrow edema associated with neuroarthropathy of the tarsal bones mimics osteomyelitis. *T* talus, *CU* cuboid, *C* calcaneus, *TIB* tibia

Table 6.7 Osteomyelitis versus neuroarthropathy

	Favors osteomyelitis	Favors neuroarthropathy
Radiography		
Location	Forefoot, metatarsal heads, and toes	Mid foot
Cortical destruction	Discrete cortical lesion	Absent
Proximity to soft tissue ulcer	Beneath or close to the ulcer or soft tissue infection	Some distance from soft tissue infection or ulcer
MR		
Signal characteristics of the abnormal marrow	Hyperintense STIR or T2 marrow signal (This signal pattern is nonspecific and overlaps the hyperemic form of neuroarthropathy and acute fracture)	Hypointense marrow signal on all T1, T2, and STIR sequences (This signal pattern corresponds to the hypertrophic form of neuroarthropathy)
Cysts	Not common in osteomyelitis	Well marginated cyst-like lesions, hypointense on T1 and hyperintense on T2

Imaging Algorithm: Approaches to Diagnosis of Pedal Osteomyelitis in the Diabetic Patient

A suggested algorithm for imaging pedal osteomyelitis in the diabetic patient is presented in Fig. 6.24.

Soft Tissue Ulceration Exposing Bone

When the soft tissue ulcer exposes bone, no imaging is needed to confirm the diagnosis of osteomyelitis. Radiography is appropriate to provide a baseline and to document bone complications

Soft Tissue Inflammation (Ulcers and/or Cellulitis) with No Exposed Bone

Radiographic findings are used to further separate the patients into two groups. If the radiographs are normal and the clinical suspicion for osteomyelitis is high, a three phase bone scan can effectively detect or exclude osteomyelitis. MRI or labeled leukocyte study is an acceptable alternative [24]. A gallium scan may replace labeled leukocyte study if the latter is not available [125]. Unlike plain radiographs, these modalities should become positive in the first few days of infection. In light of their high sensitivity, these studies provide a high negative predictive value for osteomyelitis. If the bone scan is equivocal, supplementary imaging with either MRI or labeled leukocyte scans is required.

When the radiographs are abnormal, showing neuroarthropathic, degenerative, or traumatic changes, either labeled leukocyte scan or MRI is acceptable. The choice depends on the location of the suspected osteomyelitis. If the inflammation is in the forefoot, an indium leukocyte study efficiently identifies osteomyelitis. By contrast, when the infection is in the mid- or hindfoot, MRI adequately separates bone from soft tissue inflammation.

Conclusion

Imaging plays an important role in the assessment of the diabetic patient with foot problems. Nuclear medicine and MRI techniques detect osteomyelitis, characterize various soft tissue abnormalities, and depict the extent of bone involvement. Digital subtraction angiography and noninvasive angiographic studies can be used in complementary fashion to evaluate lower extremity arterial anatomy and pathology. Nevertheless, distinguishing osteomyelitis from coincident neuropathic change remains a challenge. Only with an understanding

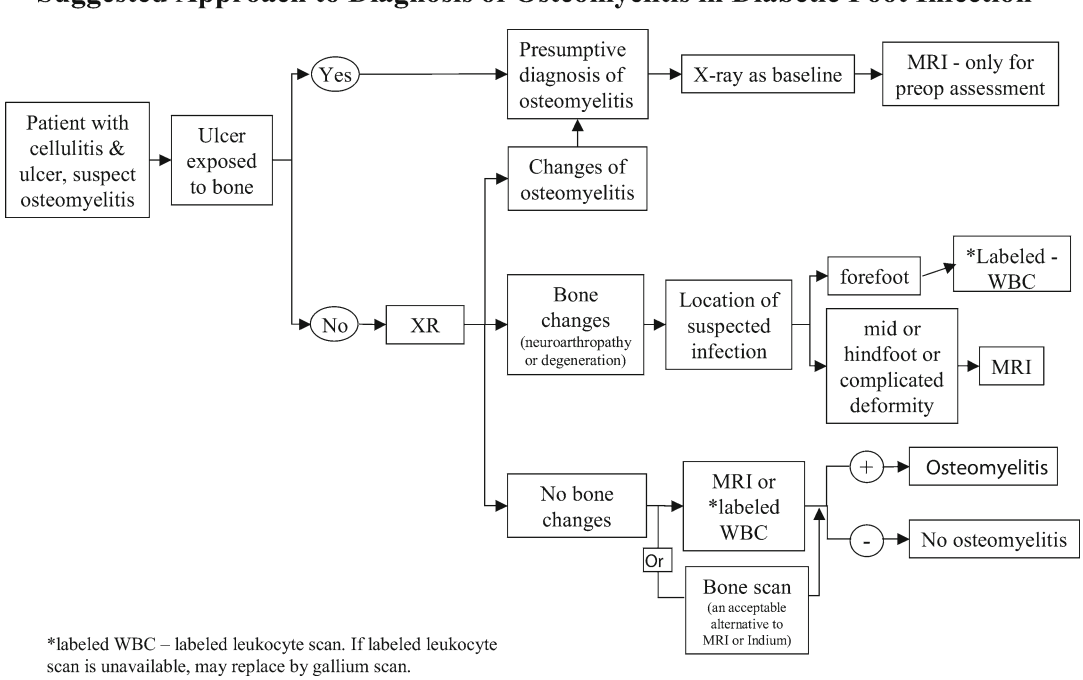

Fig. 6.24 Suggested approach to diagnosis of osteomyelitis in diabetic foot infection. (*Asterisk*) Labeled WBC refers to a labeled leukocyte scan. If labeled leukocyte scan is unavailable, may replace with gallium scan

of the specific strengths and weaknesses of each modality, as they apply to the particular clinical problem in question, can this wide variety of imaging studies be utilized in an effective and efficient manner.

Acknowledgments Sincere thanks to Drs. Yvonne Cheung, J. Anthony Parker, and David Brophy for their contributions. Thanks as well to Ms. Clotell Forde for her assistance in the preparation of this manuscript.

References

1. Newman LG, Waller J, Palestro CJ, et al. Unsuspected osteomyelitis in diabetic foot ulcers. Diagnosis and monitoring by leukocyte scanning with indium in 111 oxyquinoline. JAMA. 1991;266:1246–51.
2. Scher KS, Steele FJ. The septic foot in patients with diabetes. Surgery. 1988;104:661–6.
3. Kaufman MW, Bowsher JE. Preventing diabetic foot ulcers. Medsurg Nurs. 1994;3:204–10.
4. Bild DE, Selby JV, Sinnock P, Browner WS, Braveman P, Showstack JA. Lower-extremity amputation in people with diabetes. Epidemiology and prevention. Diabetes Care. 1989;12:24–31.
5. Ecker ML, Jacobs BS. Lower extremity amputation in diabetic patients. Diabetes. 1970;19:189–95.
6. Penn I. Infectins in the diabetic foot. In: Sammarco GJ, editor. The foot in diabetes. Philadelphia: Lea & Febiger; 1991. p. 106–23.
7. Gold RH, Tong DJ, Crim JR, Seeger LL. Imaging the diabetic foot. Skeletal Radiol. 1995;24:563–71.
8. American Diabetes Association. Economic costs of diabetes in the U.S. Diabetes Care. 2008;31:596–615.
9. Horowitz JD, Durham JR, Nease DB, Lukens ML, Wright JG, Smead WL. Prospective evaluation of magnetic resonance imaging in the management of acute diabetic foot infections. Ann Vasc Surg. 1993;7:44–50.
10. Edmonds ME, Roberts VC, Watkins PJ. Blood flow in the diabetic neuropathic foot. Diabetologia. 1982;22:9–15.
11. Murray HJ, Young MJ, Hollis S, Boulton AJ. The association between callus formation, high pressures and neuropathy in diabetic foot ulceration. Diabet Med. 1996;13:979–82.
12. Gooding GA, Stess RM, Graf PM, Moss KM, Louie KS, Grunfeld C. Sonography of the sole of the foot. Evidence for loss of foot pad thickness in diabetes and its relationship to ulceration of the foot. Invest Radiol. 1986;21:45–8.
13. Bamberger DM, Daus GP, Gerding DN. Osteomyelitis in the feet of diabetic patients. Long-term results,

prognostic factors, and the role of antimicrobial and surgical therapy. Am J Med. 1987;83:653–60.
14. Linklater J, Potter HG. Emergent musculoskeletal magnetic resonance imaging. Top Magn Reson Imaging. 1998;9:238–60.
15. Marcus CD, Ladam-Marcus VJ, Leone J, Malgrange D, Bonnet-Gausserand FM, Menanteau BP. MR imaging of osteomyelitis and neuropathic osteoarthropathy in the feet of diabetics. Radiographics. 1996;16:1337–48.
16. Moore TE, Yuh WT, Kathol MH, el-Khoury GY, Corson JD. Abnormalities of the foot in patients with diabetes mellitus: findings on MR imaging. AJR Am J Roentgenol. 1991;157:813–6.
17. Grayson ML, Gibbons GW, Balogh K, Levin E, Karchmer AW. Probing to bone in infected pedal ulcers. A clinical sign of underlying osteomyelitis in diabetic patients. JAMA. 1995;273:721–3.
18. Cook TA, Rahim N, Simpson HC, Galland RB. Magnetic resonance imaging in the management of diabetic foot infection. Br J Surg. 1996;83:245–8.
19. Wrobel JS, Connolly JE. Making the diagnosis of osteomyelitis. The role of prevalence. J Am Podiatr Med Assoc. 1998;88:337–43.
20. Dinh MT, Abad CL, Safdar N. Diagnostic accuracy of the physical examination and imaging tests for osteomyelitis underlying diabetic foot ulcers: meta-analysis. Clin Infect Dis. 2008;47:519–27.
21. Smith CD, Bilmen JG, Iqbal S, Robey S, Pereira M. Medial artery calcification as an indicator of diabetic peripheral vascular disease. Foot Ankle Int. 2008;29:185–90.
22. Bonakdar-pour A, Gaines VD. The radiology of osteomyelitis. Orthop Clin North Am. 1983;14: 21–37.
23. Schauwecker DS. The scintigraphic diagnosis of osteomyelitis. AJR Am J Roentgenol. 1992;158: 9–18.
24. Schweitzer ME, Daffner RH, Weissman BN, et al. ACR Appropriateness Criteria on suspected osteomyelitis in patients with diabetes mellitus. J Am Coll Radiol. 2008;5:881–6.
25. Palestro CJ, Love C, Miller TT. Infection and musculoskeletal conditions: imaging of musculoskeletal infections. Best Pract Res Clin Rheumatol. 2006;20: 1197–218.
26. Keenan AM, Tindel NL, Alavi A. Diagnosis of pedal osteomyelitis in diabetic patients using current scintigraphic techniques. Arch Intern Med. 1989;149: 2262–6.
27. Larcos G, Brown ML, Sutton RT. Diagnosis of osteomyelitis of the foot in diabetic patients: value of 111In-leukocyte scintigraphy. AJR Am J Roentgenol. 1991;157:527–31.
28. McCarthy K, Velchik MG, Alavi A, Mandell GA, Esterhai JL, Goll S. Indium-111-labeled white blood cells in the detection of osteomyelitis complicated by a pre-existing condition. J Nucl Med. 1988;29: 1015–21.
29. Maurer AH, Millmond SH, Knight LC, et al. Infection in diabetic osteoarthropathy: use of indium-labeled leukocytes for diagnosis. Radiology. 1986;161:221–5.
30. Splittgerber GF, Spiegelhoff DR, Buggy BP. Combined leukocyte and bone imaging used to evaluate diabetic osteoarthropathy and osteomyelitis. Clin Nucl Med. 1989;14:156–60.
31. Schauwecker DS, Park HM, Burt RW, Mock BH, Wellman HN. Combined bone scintigraphy and indium-111 leukocyte scans in neuropathic foot disease. J Nucl Med. 1988;29:1651–5.
32. Seabold JE, Flickinger FW, Kao SC, et al. Indium-111-leukocyte/technetium-99 m-MDP bone and magnetic resonance imaging: difficulty of diagnosing osteomyelitis in patients with neuropathic osteoarthropathy. J Nucl Med. 1990;31:549–56.
33. Palestro CJ, Torres MA. Radionuclide imaging in orthopedic infections. Semin Nucl Med. 1997;27:334–45.
34. Abreu SH. Skeletal uptake of indium 111-labeled white blood cells. Semin Nucl Med. 1989;19: 152–5.
35. Losbona R, Rosenthall L. Observations on the sequential use of 99mTc-phosphate complex and 67 Ga imaging in osteomyelitis, cellulitis, and septic arthritis. Radiology. 1977;123:123–9.
36. Tumeh SS, Aliabadi P, Weissman BN, McNeil BJ. Chronic osteomyelitis: bone and gallium scan patterns associated with active disease. Radiology. 1986;158:685–8.
37. Schober O, Heindel W. PET-CT hybrid imaging. Stuttgart: Thieme; 2010.
38. Keidar Z, Militianu D, Melamed E, Bar-Shalom R, Israel O. The diabetic foot: initial experience with 18 F-FDG PET/CT. J Nucl Med. 2005;46:444–9.
39. Chacko TK, Zhuang H, Nakhoda KZ, Moussavian B, Alavi A. Applications of fluorodeoxyglucose positron emission tomography in the diagnosis of infection. Nucl Med Commun. 2003;24:615–24.
40. Meller J, Koster G, Liersch T, et al. Chronic bacterial osteomyelitis: prospective comparison of (18)F-FDG imaging with a dual-head coincidence camera and (111)In-labelled autologous leucocyte scintigraphy. Eur J Nucl Med Mol Imaging. 2002;29:53–60.
41. Zhuang H, Alavi A. 18-Fluorodeoxyglucose positron emission tomographic imaging in the detection and monitoring of infection and inflammation. Semin Nucl Med. 2002;32:47–59.
42. Termaat MF, Raijmakers PG, Scholten HJ, Bakker FC, Patka P, Haarman HJ. The accuracy of diagnostic imaging for the assessment of chronic osteomyelitis: a systematic review and meta-analysis. J Bone Joint Surg Am. 2005;87:2464–71.
43. Schmitz A, Risse HJ, Kalicke T, Grunwald F, Schmitt O. FDG-PET for diagnosis and follow-up of inflammatory processes: initial results from the orthopedic viewpoint. Z Orthop Ihre Grenzgeb. 2000;138:407–12.

44. Kalicke T, Schmitz A, Risse JH, et al. Fluorine-18 fluorodeoxyglucose PET in infectious bone diseases: results of histologically confirmed cases. Eur J Nucl Med. 2000;27:524–8.
45. Hopfner S, Krolak C, Kessler S, et al. Preoperative imaging of Charcot neuroarthropathy in diabetic patients: comparison of ring PET, hybrid PET, and magnetic resonance imaging. Foot Ankle Int. 2004; 25:890–5.
46. Schwegler B, Stumpe KD, Weishaupt D, et al. Unsuspected osteomyelitis is frequent in persistent diabetic foot ulcer and better diagnosed by MRI than by 18 F-FDG PET or 99mTc-MOAB. J Intern Med. 2008;263:99–106.
47. Hara T, Higashi T, Nakamoto Y, et al. Significance of chronic marked hyperglycemia on FDG-PET: is it really problematic for clinical oncologic imaging? Ann Nucl Med. 2009;23:657–69.
48. Boutin RD, Brossmann J, Sartoris DJ, Reilly D, Resnick D. Update on imaging of orthopedic infections. Orthop Clin North Am. 1998;29:41–66.
49. Pomposelli F. Arterial imaging in patients with lower extremity ischemia and diabetes mellitus. J Vasc Surg. 2010;52:81S–91S.
50. Smith DC, Yahiku PY, Maloney MD, Hart KL. Three new low-osmolality contrast agents: a comparative study of patient discomfort. AJNR Am J Neuroradiol. 1988;9:137–9.
51. Waybill MM, Waybill PN. Contrast media-induced nephrotoxicity: identification of patients at risk and algorithms for prevention. J Vasc Interv Radiol. 2001;12:3–9.
52. Solomon R, Werner C, Mann D, D'Elia J, Silva P. Effects of saline, mannitol, and furosemide to prevent acute decreases in renal function induced by radiocontrast agents. N Engl J Med. 1994;331: 1416–20.
53. Sartoris DJ. Cross-sectional imaging of the diabetic foot. J Foot Ankle Surg. 1994;33:531–45.
54. Sartoris DJ, Devine S, Resnick D, et al. Plantar compartmental infection in the diabetic foot. The role of computed tomography. Invest Radiol. 1985; 20:772–84.
55. Gold RH, Hawkins RA, Katz RD. Bacterial osteomyelitis: findings on plain radiography, CT, MR, and scintigraphy. AJR Am J Roentgenol. 1991;157: 365–70.
56. Chandnani VP, Beltran J, Morris CS, et al. Acute experimental osteomyelitis and abscesses: detection with MR imaging versus CT. Radiology. 1990;174: 233–6.
57. Magid D, Fishman EK. Musculoskeletal infections in patients with AIDS: CT findings. AJR Am J Roentgenol. 1992;158:603–7.
58. van Holsbeeck MT, Introcaso JH. Musculoskeletal ultrasound. St. Louis: Mosby; 2001.
59. Pineda C, Espinosa R, Pena A. Radiographic imaging in osteomyelitis: the role of plain radiography, computed tomography, ultrasonography, magnetic resonance imaging, and scintigraphy. Semin Plast Surg. 2009;23:80–9.
60. Riebel TW, Nasir R, Nazarenko O. The value of sonography in the detection of osteomyelitis. Pediatr Radiol. 1996;26:291–7.
61. Cardinal E, Bureau NJ, Aubin B, Chhem RK. Role of ultrasound in musculoskeletal infections. Radiol Clin North Am. 2001;39:191–201.
62. Howard CB, Einhorn M, Dagan R, Nyska M. Ultrasound in diagnosis and management of acute haematogenous osteomyelitis in children. J Bone Joint Surg Br. 1993;75:79–82.
63. Kaiser S, Rosenborg M. Early detection of subperiosteal abscesses by ultrasonography. A means for further successful treatment in pediatric osteomyelitis. Pediatr Radiol. 1994;24:336–9.
64. Howard CB, Einhorn M, Dagan R, Nyska M. Ultrasonic features of acute osteomyelitis. J Bone Joint Surg Br. 1995;77:663–4.
65. Chao HC, Kong MS, Lin TY, Chiu CH, Wang CR, Lee ZL. Sonographic and color Doppler sonographic diagnosis of acute osteomyelitis: report of one case. Acta Paediatr Taiwan. 1999;40:268–70.
66. Enderle MD, Coerper S, Schweizer HP, et al. Correlation of imaging techniques to histopathology in patients with diabetic foot syndrome and clinical suspicion of chronic osteomyelitis. The role of high-resolution ultrasound. Diabetes Care. 1999; 22:294–9.
67. Steiner GM, Sprigg A. The value of ultrasound in the assessment of bone. Br J Radiol. 1992;65:589–93.
68. Bray PW, Mahoney JL, Campbell JP. Sensitivity and specificity of ultrasound in the diagnosis of foreign bodies in the hand. J Hand Surg Am. 1995;20: 661–6.
69. Boyse TD, Fessell DP, Jacobson JA, Lin J, van Holsbeeck MT, Hayes CW. US of soft-tissue foreign bodies and associated complications with surgical correlation. Radiographics. 2001;21:1251–6.
70. Duffin AC, Lam A, Kidd R, Chan AK, Donaghue KC. Ultrasonography of plantar soft tissues thickness in young people with diabetes. Diabet Med. 2002;19:1009–13.
71. Hsu TC, Wang CL, Shau YW, Tang FT, Li KL, Chen CY. Altered heel-pad mechanical properties in patients with Type 2 diabetes mellitus. Diabet Med. 2000;17:854–9.
72. Morrison WB, Schweitzer ME, Wapner KL, Hecht PJ, Gannon FH, Behm WR. Osteomyelitis in feet of diabetics: clinical accuracy, surgical utility, and cost-effectiveness of MR imaging. Radiology. 1995;196: 557–64.
73. Wertman R, Altun E, Martin DR, et al. Risk of nephrogenic systemic fibrosis: evaluation of gadolinium chelate contrast agents at four American universities. Radiology. 2008;248:799–806.
74. Broome DR, Girguis MS, Baron PW, Cottrell AC, Kjellin I, Kirk GA. Gadodiamide-associated nephrogenic systemic fibrosis: why radiologists should

be concerned. AJR Am J Roentgenol. 2007;188: 586–92.
75. Sena BF, Stern JP, Pandharipande PV, et al. Screening patients to assess renal function before administering gadolinium chelates: assessment of the Choyke questionnaire. AJR Am J Roentgenol. 2010;195: 424–8.
76. http://www.fda.gov/Safety/MedWatch/SafetyInformation/SafetyAlertsforHumanMedicalProducts/ucm225375.htm.
77. Miller TT, Randolph Jr DA, Staron RB, Feldman F, Cushin S. Fat-suppressed MRI of musculoskeletal infection: fast T2-weighted techniques versus gadolinium-enhanced T1-weighted images. Skeletal Radiol. 1997;26:654–8.
78. Morrison WB, Schweitzer ME, Batte WG, Radack DP, Russel KM. Osteomyelitis of the foot: relative importance of primary and secondary MR imaging signs. Radiology. 1998;207:625–32.
79. Horowitz SH. Diabetic neuropathy. Clin Orthop Relat Res. 1993;296:78–85.
80. Nigro ND, Bartynski WS, Grossman SJ, Kruljac S. Clinical impact of magnetic resonance imaging in foot osteomyelitis. J Am Podiatr Med Assoc. 1992;82:603–15.
81. Wang A, Weinstein D, Greenfield L, et al. MRI and diabetic foot infections. Magn Reson Imaging. 1990;8:805–9.
82. Yu JS. Diabetic foot and neuroarthropathy: magnetic resonance imaging evaluation. Top Magn Reson Imaging. 1998;9:295–310.
83. Weinstein D, Wang A, Chambers R, Stewart CA, Motz HA. Evaluation of magnetic resonance imaging in the diagnosis of osteomyelitis in diabetic foot infections. Foot Ankle. 1993;14:18–22.
84. Beltran J, Campanini DS, Knight C, McCalla M. The diabetic foot: magnetic resonance imaging evaluation. Skeletal Radiol. 1990;19:37–41.
85. Berquist TH. Infection. In: Berquist TH, editor. Imaging of the foot and ankle. Philadelphia: Wolters Kluwer/Lippincott Williams & Wilkins; 2011. p. 436–86.
86. Ledermann HP, Schweitzer ME, Morrison WB. Nonenhancing tissue on MR imaging of pedal infection: characterization of necrotic tissue and associated limitations for diagnosis of osteomyelitis and abscess. AJR Am J Roentgenol. 2002;178: 215–22.
87. Bus SA, Maas M, Cavanagh PR, Michels RP, Levi M. Plantar fat-pad displacement in neuropathic diabetic patients with toe deformity: a magnetic resonance imaging study. Diabetes Care. 2004;27: 2376–81.
88. Andreassen CS, Jakobsen J, Ringgaard S, Ejskjaer N, Andersen H. Accelerated atrophy of lower leg and foot muscles—a follow-up study of long-term diabetic polyneuropathy using magnetic resonance imaging (MRI). Diabetologia. 2009;52:1182–91.
89. Brash PD, Foster J, Vennart W, Anthony P, Tooke JE. Magnetic resonance imaging techniques demonstrate soft tissue damage in the diabetic foot. Diabet Med. 1999;16:55–61.
90. Dinh T, Doupis J, Lyons TE, et al. Foot muscle energy reserves in diabetic patients without and with clinical peripheral neuropathy. Diabetes Care. 2009;32:1521–4.
91. Greenman RL, Panasyuk S, Wang X, et al. Early changes in the skin microcirculation and muscle metabolism of the diabetic foot. Lancet. 2005;366: 1711–7.
92. Suzuki E, Kashiwagi A, Hidaka H, et al. 1 H- and 31P-magnetic resonance spectroscopy and imaging as a new diagnostic tool to evaluate neuropathic foot ulcers in Type II diabetic patients. Diabetologia. 2000;43:165–72.
93. Weaver JB, Doyley M, Cheung Y, et al. Imaging the shear modulus of the heel fat pads. Clin Biomech (Bristol, Avon). 2005;20:312–9.
94. Pomposelli Jr FB, Marcaccio EJ, Gibbons GW, et al. Dorsalis pedis arterial bypass: durable limb salvage for foot ischemia in patients with diabetes mellitus. J Vasc Surg. 1995;21:375–84.
95. Sze DY. Conventional angiography in the noninvasive era. In: Rubin Geoffrey D, Rofsky NM, editors. CT and MR angiography: comprehensive vascular assessment. Philadelphia: Wolters Kluwer/Lippincott, Williams & Wilkins; 2009. p. 87–127.
96. Lindholt JS. Radiocontrast induced nephropathy. Eur J Vasc Endovasc Surg. 2003;25:296–304.
97. Cotroneo AR, Manfredi R, Settecasi C, Prudenzano R, Di Stasi C. Angiography and MR-angiography in the diagnosis of peripheral arterial occlusive disease in diabetic patients. Rays. 1997;22:579–90.
98. Kreitner KF, Kalden P, Neufang A, et al. Diabetes and peripheral arterial occlusive disease: prospective comparison of contrast-enhanced three-dimensional MR angiography with conventional digital subtraction angiography. AJR Am J Roentgenol. 2000;174:171–9.
99. Meaney JF. Magnetic resonance angiography of the peripheral arteries: current status. Eur Radiol. 2003;13:836–52.
100. Sharafuddin MJ, Stolpen AH, Sun S, et al. High-resolution multiphase contrast-enhanced three-dimensional MR angiography compared with two-dimensional time-of-flight MR angiography for the identification of pedal vessels. J Vasc Interv Radiol. 2002;13:695–702.
101. Berquist TH, Adelson AB. Bone and soft tissue ischemia. In: Berquist TH, editor. Imaging of the foot and ankle. Philadelphia: Wolters Kluwer/Lippincott Williams & Wilkins; 2011. p. 375–435.
102. Herborn CU, Goyen M, Quick HH, et al. Whole-body 3D MR angiography of patients with peripheral arterial occlusive disease. AJR Am J Roentgenol. 2004;182:1427–34.
103. Owen RS, Carpenter JP, Baum RA, Perloff LJ, Cope C. Magnetic resonance imaging of angiographically occult runoff vessels in peripheral arterial occlusive disease. N Engl J Med. 1992;326:1577–81.

104. Leiner T, Fleischmann D, Rofsky NM. Conventional angiography in the noninvasive era. In: Rubin GD, Rofsky NM, editors. CT and MR angiography: comprehensive vascular assessment. Philadelphia: Wolters Kluwer/Lippincott, Williams & Wilkins; 2009. p. 921–1016.
105. Nelemans PJ, Leiner T, de Vet HC, van Engelshoven JM. Peripheral arterial disease: meta-analysis of the diagnostic performance of MR angiography. Radiology. 2000;217:105–14.
106. Dorweiler B, Neufang A, Kreitner KF, Schmiedt W, Oelert H. Magnetic resonance angiography unmasks reliable target vessels for pedal bypass grafting in patients with diabetes mellitus. J Vasc Surg. 2002;35:766–72.
107. Andros G. Diagnostic and therapeutic arterial interventions in the ulcerated diabetic foot. Diabetes Metab Res Rev. 2004;20 Suppl 1:S29–33.
108. Roos JE, Hellinger JC, Hallet R, Fleischmann D, Zarins CK, Rubin GD. Detection of endograft fractures with multidetector row computed tomography. J Vasc Surg. 2005;42:1002–6.
109. Hartnell GG. Contrast angiography and MR angiography: still not optimum. J Vasc Interv Radiol. 1999;10:99–100.
110. Brenner DJ, Hall EJ. Computed tomography—an increasing source of radiation exposure. N Engl J Med. 2007;357:2277–84.
111. Willmann JK, Baumert B, Schertler T, et al. Aortoiliac and lower extremity arteries assessed with 16-detector row CT angiography: prospective comparison with digital subtraction angiography. Radiology. 2005;236:1083–93.
112. Ouwendijk R, Kock MC, van Dijk LC, van Sambeek MR, Stijnen T, Hunink MG. Vessel wall calcifications at multi-detector row CT angiography in patients with peripheral arterial disease: effect on clinical utility and clinical predictors. Radiology. 2006;241:603–8.
113. Zweibel WJ, Pellerito JS. Basic concepts of Doppler frequency spectrum analysis and ultrasound blood flow imaging. In: John S, Zweibel William JP, editors. Introduction to vascular ultrasonography. Philadelphia: Elsevier Saunders; 2005. p. 61–89.
114. de Smet AA, Ermers EJ, Kitslaar PJ. Duplex velocity characteristics of aortoiliac stenoses. J Vasc Surg. 1996;23:628–36.
115. Cossman DV, Ellison JE, Wagner WH, et al. Comparison of contrast arteriography to arterial mapping with color-flow duplex imaging in the lower extremities. J Vasc Surg. 1989;10:522–8. discussion 528–9.
116. Dyet JF, Nicholson AA, Ettles DF. Vascular imaging and intervention in peripheral arteries in the diabetic patient. Diabetes Metab Res Rev. 2000;16 Suppl 1:S16–22.
117. Edwards JM, Coldwell DM, Goldman ML, Strandness Jr DE. The role of duplex scanning in the selection of patients for transluminal angioplasty. J Vasc Surg. 1991;13:69–74.
118. Larch E, Minar E, Ahmadi R, et al. Value of color duplex sonography for evaluation of tibioperoneal arteries in patients with femoropopliteal obstruction: a prospective comparison with anterograde intraarterial digital subtraction angiography. J Vasc Surg. 1997;25:629–36.
119. Hofmann WJ, Walter J, Ugurluoglu A, Czerny M, Forstner R, Magometschnigg H. Preoperative high-frequency duplex scanning of potential pedal target vessels. J Vasc Surg. 2004;39:169–75.
120. Levy MM, Baum RA, Carpenter JP. Endovascular surgery based solely on noninvasive preprocedural imaging. J Vasc Surg. 1998;28:995–1003. discussion 1003–5.
121. Beltran J. MR imaging of soft tissue infection. Magn Reson Imaging Clin N Am. 1995;3:743–51.
122. Sequeira W. The neuropathic joint. Clin Exp Rheumatol. 1994;12:325–37.
123. Zlatkin MB, Pathria M, Sartoris DJ, Resnick D. The diabetic foot. Radiol Clin North Am. 1987;25:1095–105.
124. Brower AC, Allman RM. Pathogenesis of the neurotrophic joint: neurotraumatic vs. neurovascular. Radiology. 1981;139:349–54.
125. Donohoe KJ. Selected topics in orthopedic nuclear medicine. Orthop Clin North Am. 1998;29:85–101.
126. Newman LG, Waller J, Palestro CJ, et al. Unsuspected osteomyelitis in diabetic foot ulcers. Diagnosis and monitoring by leukocyte scanning with indium in 111 oxyquinoline [see comments]. JAMA. 1991;266:1246–51.
127. Segall GM, Nino-Murcia M, Jacobs T, Chang K. The role of bone scan and radiography in the diagnostic evaluation of suspected pedal osteomyelitis. Clin Nucl Med. 1989;14:255–60.
128. Seldin DW, Heiken JP, Feldman F, Alderson PO. Effect of soft-tissue pathology on detection of pedal osteomyelitis in diabetics. J Nucl Med. 1985;26:988–93.
129. Newman LG. Imaging techniques in the diabetic foot. Clin Podiatr Med Surg. 1995;12:75–86.